

# Galactic star formation enhanced and quenched by ram pressure in groups and clusters

Kenji Bekki<sup>1\*</sup>

<sup>1</sup>*ICRAR M468 The University of Western Australia 35 Stirling Hwy, Crawley Western Australia 6009, Australia*

Accepted, Received 2005 February 20; in original form

## ABSTRACT

We investigate how ram pressure of intragroup and intracluster medium can influence the spatial and temporal variations of star formation (SF) of disk galaxies with halo masses ( $M_h$ ) ranging from  $10^{10}M_\odot$  to  $10^{12}M_\odot$  (i.e., from dwarf irregular to Milky Way-type) in groups and clusters with  $10^{13} \leq M_h/M_\odot \leq 10^{15}$  by using numerical simulations with a new model for time-varying ram pressure. The long-term evolution of SF rates and H $\alpha$  morphologies corresponding to the distributions of star-forming regions are particularly investigated for different model parameters. The principal results are as follows. Whether ram pressure can enhance or reduce SF depends on  $M_h$  of disk galaxies and inclination angles of gas disks with respect to their orbital directions for a given orbit and a given environment. For example, SF can be moderately enhanced in disk galaxies with  $M_h = 10^{12}M_\odot$  at the pericenter passages in a cluster with  $M_h = 10^{14}M_\odot$  whereas it can be completely shut down (‘quenching’) for low-mass disks with  $M_h = 10^{10}M_\odot$ . Ram pressure can reduce the H $\alpha$ -to-optical-disk-size ratios of disks and the level of the reduction depends on  $M_h$  and orbits of disk galaxies for a given environment. Disk galaxies under strong ram pressure show characteristic H $\alpha$  morphologies such as ring-like, one-sided, and crescent-like distributions.

**Key words:** galaxies: clusters : general – galaxies:ISM – galaxies:evolution – stars:formation

## 1 INTRODUCTION

Galaxy evolution in groups and clusters can be significantly influenced by environmental processes, such as tidal compression of cluster gravitational fields (e.g., Byrd & Valtonen 1990), merging between group member galaxies (e.g., Mamon 2001), ram pressure stripping of disk gas (e.g., Gunn & Gott 1972), high external pressure of intracluster medium (ICM) on galactic gas disks (e.g., Evrard 1991), multiple high-speed galaxy encounters (e.g., Moore et al. 1994), and stripping of galactic halo gas by ram pressure of ICM (e.g., Bekki 2009). One of key issues in extragalactic astronomy is to understand the relative importance of each of these environmental processes in galaxy evolution for different environments (See Boselli & Gavazzi 2006 for a recent review on this). Ram pressure effect on galactic gas disk is distinct from other environmental processes based on gravitation interaction in the sense that it can influence only the cold gaseous components of disk galaxies (i.e., it can not directly influence the stellar components). Ram pressure of ICM, however, can be a key process for better understanding the

star formation histories (SFHs) of disk galaxies in groups and clusters, as described throughout this paper.

Recent observational studies have shown that ram pressure stripping can influence temporal and spatial variations of star formation (SF) in disk galaxies (e.g., Koopmann & Kenny 2004; Crowl & Kenny 2008; Cortese et al. 2012; Fossati et al. 2013). For example, Koopmann & Kenny (2004) found that spiral galaxies with truncated H $\alpha$  disks show undisturbed stellar disks in the Virgo cluster and accordingly suggested that hydrodynamical interaction between ICM and interstellar medium (ISM) is responsible for the truncated H $\alpha$  disks. Also, these observations found that the H $\alpha$ -to-optical-disk-size ratio is smaller for spiral galaxies with higher degrees of H I-deficiency. (e.g., a negative correlation between  $r_e(\text{H}\alpha)/r_e$  and  $\text{Def}_{\text{HI}}$ ; Fossati et al. 2013). Given that the time evolution of global colors and chemical abundances of disk galaxy depends strongly on SFHs, these observations suggest that understanding the roles of ram pressure in SFHs of galaxies is important also for better understanding galaxy evolution in general.

Although many numerical simulations investigated in what physical conditions ISM of galaxies with different morphological types can be stripped by ram pressure (e.g.,

\* E-mail: bekki@cyllene.uwa.edu.au

Abadi et al. 1999; Mori & Burkert 2000; Quilis et al. 2000; Schultz & Struck 2001; Vollmer et al. 2001; Roediger & Hensler 2005; Roediger & Brüggén 2007; Jáchym et al. 2007; Kronberger et al. 2008; Tonnesen & Bryan 2012), a surprisingly small number of simulations have so far investigated how the SFHs of disk galaxies can be influenced by ram pressure. Bekki & Couch (2003) demonstrated that external high pressure of ICM on gas clouds in disk galaxies can induce the gravitational collapse of the clouds and thus can trigger a very efficient star formation (starburst). Kronberger et al. (2008) showed that ram pressure of ICM can significantly enhance (by up to a factor of 3) the mean star formation rates in the central regions of disk galaxies, if the ICM has a density of  $10^{-28}$  g cm $^{-3}$  and a temperature of  $3.6 \times 10^7$  K. Mastropietro et al. (2009) investigated how ram pressure of the Galactic halo gas can influence the distribution of star-forming regions in the Large Magellanic Cloud (LMC). Tonnesen & Bryan (2012) demonstrated that star formation in galactic bulges can be slightly enhanced in disk galaxies under moderately strong ram pressure of ICM.

Although these previous simulations clearly demonstrated that external high pressure of ICM can possibly enhance star formation in disk galaxies under some physical conditions, they did not investigate the long-term (more than a few Gyr) SFHs of galaxies under ram pressure in a systematic parameter study. Furthermore, these previous simulations did not properly model the time evolution of the strength of ram pressure for disk galaxies which enter into clusters from fields. Since the strength of ram pressure depends both on (i) the relative velocities between ICM and galaxies and on (ii) the densities of ICM surrounding galaxies, orbital evolution of galaxies within clusters needs to be included in simulating the long-term effects of ram pressure on galaxies. Accordingly, it is unclear how ram pressure can influence SFHs of galaxies when they enter into a cluster environment and passes through its central region. A more comprehensive systematic parameter study on the influences of ram pressure on SFHs of galaxies is necessary.

The purpose of this paper is to investigate how ram pressure of ICM can influence the long-term SFHs of disk galaxies in a comprehensive manner by using numerical simulations with a proper model for time-varying ram pressure force. We particularly investigate the following questions: (i) whether ram pressure can enhance or reduce star formation in disk galaxies, (ii) how the effects of ram pressure on galactic SFHs depend on galaxy properties and environments, (iii) how the H $\alpha$  distributions of disk galaxies under strong ram pressure look like, (iv) how the ratios of H $\alpha$  disk sizes to optical disk ones depend on galaxy/group/cluster masses, and (v) how ram pressure is important for better understanding the observed properties of galaxies in groups and clusters.

Given ongoing extensive observational studies of 2D H $\alpha$  distribution of star-forming regions in galaxies by multi-object spectrograph on large ground-based telescopes (e.g., Croom et al. 2012; Brough et al. 2013), it is very timely for the present study to predict 2D H $\alpha$  distributions of star-forming regions in disk galaxies under strong ram pressure. These predictions will help observers to interpret the origin of the H $\alpha$  morphologies of disk galaxies in different environments (e.g., Moss & Whittle 2000; Koopmann & Kenny 2004). Galactic SFHs in groups and clusters have been dis-

cussed in the context of gradual decline due to *halo gas* stripping ('strangulation'; Larson et al. 2002; Balogh et al. 2000; Bekki et al. 2001, 2002; Shioya et al. 2004). Ram pressure stripping of *disk gas* can cause sudden and rapid removal of gas and thus can have more dramatic effects on SFHs of galaxies in comparison with the strangulation mechanism.

The plan of the paper is as follows: In the next section, we describe our new model for time-dependent ram pressure force on disk galaxies in clusters. In §3, we present the numerical results on the long-term SFHs and spatial distributions of SF regions in disk galaxies under strong ram pressure. In this section, we also discuss the dependences of the results on the adopted model parameters. In §4, we discuss the possibly important implications of the simulations results. We summarize our conclusions in §5.

## 2 THE MODEL

A disk galaxy is assumed to move in a cluster with a total halo mass  $M_h$  and therefore be influenced by ram pressure of the ICM. The ram pressure force on the disk galaxy is calculated according to the position and velocity of the galaxy with respect to the cluster center. The tidal field of the cluster and tidal interaction with other cluster member galaxies are not included in the present study so that ram pressure effects on galactic SFHs can be more clearly investigated. Other key environmental effects on galaxies (e.g., slow and fast tidal encounters) will be investigated in our forthcoming papers. We focus exclusively on how SFHs of disk galaxies under strong ram pressure of ICM depend on galaxy properties and environments.

In order to simulate the time evolution of SFRs and gas contents in disk galaxies under ram pressure of ICM, we use our original chemodynamical simulation code that can be run on GPU machines (Bekki 2013). The code is a revised version of our original GRAPE-SPH code (Bekki 2009) which combines the method of smoothed particle hydrodynamics (SPH) with GRAPE for calculations of three-dimensional self-gravitating fluids in astrophysics. This code enable us to investigate the formation and evolution of dust and molecular hydrogen (H $_2$ ) in disk galaxies (Bekki 2013), though it is numerically costly to calculate H $_2$  formation and evolution (i.e., it requires much longer CPU time in comparison with our simulations with no H $_2$  calculation). Since our main interest is the time evolution of SFRs in galaxies (not the evolution of dust and H $_2$  contents), we do not incorporate H $_2$  calculations into the present simulation.

### 2.1 A disk galaxy

A disk galaxy is composed of dark matter halo, stellar disk, stellar bulge, and gaseous disk, as is assumed in other numerical simulations of ram pressure stripping (e.g., Abadi et al 1999; Jáchym et al. 2007). Our previous study (Bekki 2009) investigated already the ram pressure stripping of halo gas in disk galaxies within groups and clusters of galaxies. We therefore do not investigate the ram pressure stripping of halo gas by modeling halo gas in the present simulation. The total masses of dark matter halo, stellar disk, gas disk, and bulge are denoted as  $M_h$ ,  $M_s$ ,  $M_g$ , and  $M_b$ , respectively. The

**Table 1.** Description of the basic parameter values for the three different disk galaxy models.

Model name/Physical properties	MW-type	M33-type	Dwarf-type
DM mass ( $\times 10^{12} M_{\odot}$ )	1.0	0.1	0.01
Virial radius (kpc)	245.0	113.8	52.9
$c^a$	10	12	16
Stellar disk mass ( $\times 10^{10} M_{\odot}$ )	5.4	0.36	0.036
Gas disk mass ( $\times 10^{10} M_{\odot}$ )	1.2	0.3	0.03
Bulge mass ( $\times 10^{10} M_{\odot}$ )	1.0	–	–
Stellar disk size (kpc)	17.5	8.1	3.8
Gas disk size (kpc)	35.0	16.2	7.6
Bulge size (kpc)	3.5	–	–

<sup>a</sup>  $c$  is the  $c$ -parameter in the NFW dark matter profiles.

total disk mass (gas + stars) and gas mass fraction are denoted as  $M_d$  and  $f_g$ , respectively, for convenience. The mass ratio of the dark matter halo ( $M_h$ ) to the disk ( $M_s + M_g$ ) in a disk galaxy is fixed at 16.7.

We mainly investigate three different disk galaxy models with different  $M_h$  in order to clarify how a galaxy environment can influence different types of galaxies in a different manner. The three includes the ‘MW-type’ (labeled as ‘MW’ for simplicity) with  $M_h = 10^{12} M_{\odot}$ , ‘M33-type’ (‘M33’) with  $M_h = 10^{11} M_{\odot}$ , and ‘Dwarf-type’ (‘DW’), with  $M_h = 10^{10} M_{\odot}$ . These three disk models have physical properties which are similar to yet not exactly the same as those observed for the MW, M33, and typical dwarfs. These name are used just for distinguishing three disk galaxies with different  $M_h$ . The MW-type galaxy has a bulge and a smaller gas mass fraction whereas the other two have no bulge and a larger gas mass fraction. The basic parameter values for these three disk models are summarized in Table 1.

We adopt the density distribution of the NFW halo (Navarro, Frenk & White 1996) suggested from CDM simulations:

$$\rho(r) = \frac{\rho_0}{(r/r_s)(1+r/r_s)^2}, \quad (1)$$

where  $r$ ,  $\rho_0$ , and  $r_s$  are the spherical radius, the characteristic density of a dark halo, and the scale length of the halo, respectively. The  $c$ -parameter ( $c = r_{\text{vir}}/r_s$ , where  $r_{\text{vir}}$  is the virial radius of a dark matter halo) and  $r_{\text{vir}}$  are chosen appropriately for a given dark halo mass ( $M_{\text{dm}}$ ) by using the  $c - M_h$  relation predicted by recent cosmological simulations (Neto et al. 2007).

The bulge of a disk galaxy (for the MW-type) has a size of  $R_b$  and a scale-length of  $R_{0,b}$  and is represented by the Hernquist density profile. The bulge is assumed to have isotropic velocity dispersion and the radial velocity dispersion is given according to the Jeans equation for a spherical system. Although the bulge-mass fraction ( $f_b = M_b/M_d$ ) can be a free parameter, we mainly investigate the MW-type models with  $f_b = 0.17$  and  $R_b = 0.2R_s$  (i.e.,  $R_{0,b} = 0.04R_s$ ).

The radial ( $R$ ) and vertical ( $Z$ ) density profiles of the stellar disk are assumed to be proportional to  $\exp(-R/R_0)$  with scale length  $R_0 = 0.2R_s$  and to  $\text{sech}^2(Z/Z_0)$  with scale length  $Z_0 = 0.04R_s$ , respectively. The gas disk with a size  $R_g = 2R_s$  has the radial and vertical scale lengths of  $0.2R_g$  and  $0.02R_g$ , respectively. In the present model for the MW-type, the exponential disk has  $R_s = 17.5$  kpc and  $R_g = 35$  kpc. In addition to the rotational velocity caused by the

gravitational field of disk, bulge, and dark halo components, the initial radial and azimuthal velocity dispersions are assigned to the disc component according to the epicyclic theory with Toomre’s parameter  $Q = 1.5$ . The vertical velocity dispersion at a given radius is set to be 0.5 times as large as the radial velocity dispersion at that point.

Although the present simulation code enables us to investigate the time evolution of chemical abundances and dust properties in a self-consistent manner, we do not investigate these properties in the present study. This is firstly because we focus exclusively on SFHs of disk galaxies (i.e., not chemical evolution), and secondly because inclusion of such calculations of chemical and dust evolution is numerically costly and not suitable for a wide parameter study like the present work. We therefore investigate only dynamical and hydrodynamical evolution of galaxies with star formation in the present study. Initial temperature of gas is set to be  $10^4$  K for all models.

The total numbers of particles used for dark matter, stellar disk, gas disk, and bulge in a MW-type disk are 700000, 200000, 100000, and 33400, respectively (i.e.,  $N = 1033400$  is used in total). Since no bulge is included in the M33-type and Dwarf-type models, the total particle number is 1000000 for the two. The softening length of dark matter halo ( $\epsilon_{\text{dm}}$ ) for each model is chosen so that  $\epsilon_{\text{dm}}$  can be the same as the mean particle separation at the half-mass radius of the halo. This method is applied for determining softening length for stellar particles ( $\epsilon_s$ ) in the initial disk of each model. The softening length is assumed to be the same between old stellar, gaseous, and new stellar particles in the present study. The gravitational softening length for dark ( $\epsilon_{\text{dm}}$ ) and baryonic components ( $\epsilon_s$ ) are 2.1 kpc and 200 pc, respectively, for the MW-type disk. These values are different in models with different sizes and masses. In Appendix A, we discuss how the present results depend on the resolution of simulations, in particular, the total particle number used for a disk galaxy,  $N_d$ .

## 2.2 Star formation and SN feedback effects

A gas particle *can be* converted into a new star if (i) the local dynamical time scale is shorter than the sound crossing time scale (mimicking the Jeans instability), (ii) the local velocity field is identified as being consistent with gravitationally collapsing (i.e.,  $\text{div } \mathbf{v} < 0$ ), and (iii) the local density exceeds a threshold density for star formation ( $\rho_{\text{th}}$ ). The threshold

**Table 2.** Description of the basic parameter values for the three different disk galaxy models.

Model/Physical properties	Group <sup>a</sup>	Low-mass cluster ('Virgo')	High-mass cluster ('Coma')
Total mass ( $\times 10^{14} M_{\odot}$ )	0.1	1.0	10.0
Virial radius (Mpc)	0.56	1.20	2.59
<sup>c</sup> <sup>b</sup>	6.0	4.9	3.6
ICM mass ( $\times 10^{14} M_{\odot}$ )	0.015	0.15	1.5
ICM temperature ( $\times 10^7$ K)	0.56	2.6	12.0

<sup>a</sup> These definition of 'Group', 'Low-mass cluster', and 'High-mass cluster' by mass ( $M_h$ ) would be arbitrary.

<sup>b</sup> <sup>c</sup> is the  $c$ -parameter in the NFW dark matter profiles.

gas density is given in units of the number of hydrogen atoms per  $\text{cm}^3$  in the present study just for convenience. Accordingly,  $\rho_{\text{th}} = 1 \text{ cm}^{-3}$  indeed means  $\rho_{\text{th}} = 1 m_{\text{H}} \text{ cm}^{-3}$ , where  $m_{\text{H}}$  is the mass of a hydrogen atom. We mainly investigate the models with  $\rho_{\text{th}} = 1 \text{ cm}^{-3}$ , and the dependences of the present results on  $\rho_{\text{th}}$  are briefly discussed in §3.6.

A gas particle can be regarded as a 'SF candidate' gas particle if the above three SF conditions (i)-(iii) are satisfied. It could be possible to convert some fraction of a SF candidate gas particle into a new star at each time step until the mass of the gas particle becomes very small. However, this SF conversion method can increase dramatically the total number of stellar particles, which becomes numerically very costly. We therefore adopt the following SF conversion method that was already adopted by our previous chemodynamical simulations of galaxies (Bekki & Shioya 1998). A SF candidate  $i$ -th gas particle is regarded as having a SF probability ( $P_{\text{sf}}$ );

$$P_{\text{sf}} = 1 - \exp(-\Delta t \rho^{\alpha_{\text{sf}}}), \quad (2)$$

where  $\Delta t$  is the time step width for the gas particle,  $\rho$  is the gas density of the particle, and  $\alpha_{\text{sf}}$  is the power-law slope of the Kennicutt-Schmidt law ( $\text{SFR} \propto \rho_{\text{g}}^{\alpha_{\text{sf}}}$ ; Kennicutt 1998). A reasonable value of  $\alpha_{\text{sf}} = 1.5$  is adopted in the present study.

At each time step random numbers ( $R_{\text{sf}}; 0 \leq R_{\text{sf}} \leq 1$ ) are generated and compared with  $P_{\text{sf}}$ . If  $R_{\text{sf}} < P_{\text{sf}}$ , then the gas particle can be converted into a new stellar one. In this SF recipe, a gas particle with a higher gas density and thus a shorter SF timescale ( $\propto \rho/\dot{\rho} \propto \rho^{1-\alpha_{\text{sf}}}$ ) can be more rapidly converted into a new star owing to the larger  $P_{\text{sf}}$ . We thus consider that the present SF model is a good approximation for star formation in high-density gas of disk galaxies.

Each SN is assumed to eject the feedback energy ( $E_{\text{sn}}$ ) of  $10^{51}$  erg and 90% and 10% of  $E_{\text{sn}}$  are used for the increase of thermal energy ('thermal feedback') and random motion ('kinematic feedback'), respectively. The thermal energy is used for the 'adiabatic expansion phase', where each SN can remain adiabatic for a timescale of  $t_{\text{adi}}$ . Although a reasonable value for a single SN explosion is  $t_{\text{adi}} = 10^5$  yr, we adopt  $t_{\text{adi}} = 10^6$  yr in the present study, because  $t_{\text{adi}}$  might be much longer for multiple SN explosions in a small local region owing to complicated interaction between gaseous ejecta from different SNe. The energy-ratio of thermal to kinematic feedback is consistent with previous numerical simulations by Thornton et al. (1998) who investigated the energy conversion processes of SNe in detail. The way to distribute  $E_{\text{sn}}$  of SNe among neighbor gas particles is the same as described in Bekki (2013). The radiative cooling

processes are properly included by using the cooling curve by Rosen & Bregman (1995) for  $100 \leq T < 10^4 \text{ K}$  and the MAPPING III code for  $T \geq 10^4 \text{ K}$  (Sutherland & Dopita 1993).

## 2.3 Time-varying ram pressure force

### 2.3.1 A box of ICM

A disk galaxy is assumed to be embedded in hot ICM with temperature  $T_{\text{ICM}}$ , density  $\rho_{\text{ICM}}$ , and velocity  $V_r$ . Here  $V_r$  is the relative velocity of ICM with respect to the velocity of the disk galaxy. The intragroup medium in groups is also referred to as ICM just for convenience in the present study. The strength of ram pressure force on the disk is time-dependent and described as follows:

$$P_{\text{ram}}(t) = \rho_{\text{ICM}}(t) V_r^2(t), \quad (3)$$

where  $\rho_{\text{ICM}}(t)$  and  $V_r(t)$  are determined by 3D positions and velocities of a galaxy at each time step in a simulation (described later).

In order to avoid huge particle numbers to represent the entire ICM in clusters of galaxies (e.g., Abadi et al. 1999), the ICM is represented by SPH particles in a cube with the size of  $R_{\text{ICM}}$ . A disk galaxy is placed in the exact center of the cube and the direction of the orbit (within a cluster) is chosen as the  $x$ -axis in the Cartesian coordinate of the cube (Therefore, it should be noted that this  $x$ -axis is not the same as the  $x$ -axis in the orbital calculation of the present study shown in Fig. 1). The ICM cube is represented by  $60^3$  SPH particles each of which is on the  $60 \times 60 \times 60$  cubic lattice. The initial velocity of each SPH particle for the ICM is set to be ( $V_r(t=0), 0, 0$ ) for all models (i.e., the particle flows along the  $x$ -axis to the positive  $x$  direction). The ICM has an uniform distribution within the cube and  $R_{\text{ICM}}$  is set to be  $6R_s$ , and  $T_{\text{ICM}}$  is much higher than the temperature of cold ISM in galaxies. We include periodic boundary conditions (at  $R_{\text{ICM}}$ ) for the ICM SPH particles leaving the cube. In Appendix A, we briefly discuss how the present results depend on the total number of ICM particles ( $N_{\text{ICM}}$ ) and the box size ( $R_{\text{ICM}}$ ).

The strength of ram pressure of ICM depend on  $\rho_{\text{ICM}}(t)$  and  $V_r(t)$ , but it does not depend explicitly on  $T_{\text{ICM}}$ . Furthermore, the present study focuses on the influences of ram pressure on galaxy evolution in groups and clusters with  $M_h \geq 10^{13} M_{\odot}$  with high ICM temperature ( $> 10^6 \text{ K}$ ). We therefore assume that  $T_{\text{ICM}}$  is fixed at a certain value for a cluster (no radial temperature gradient and no temporal variation for simplicity) and determined by the initial total halo mass of the cluster ( $M_h$ ). We investigate two cluster

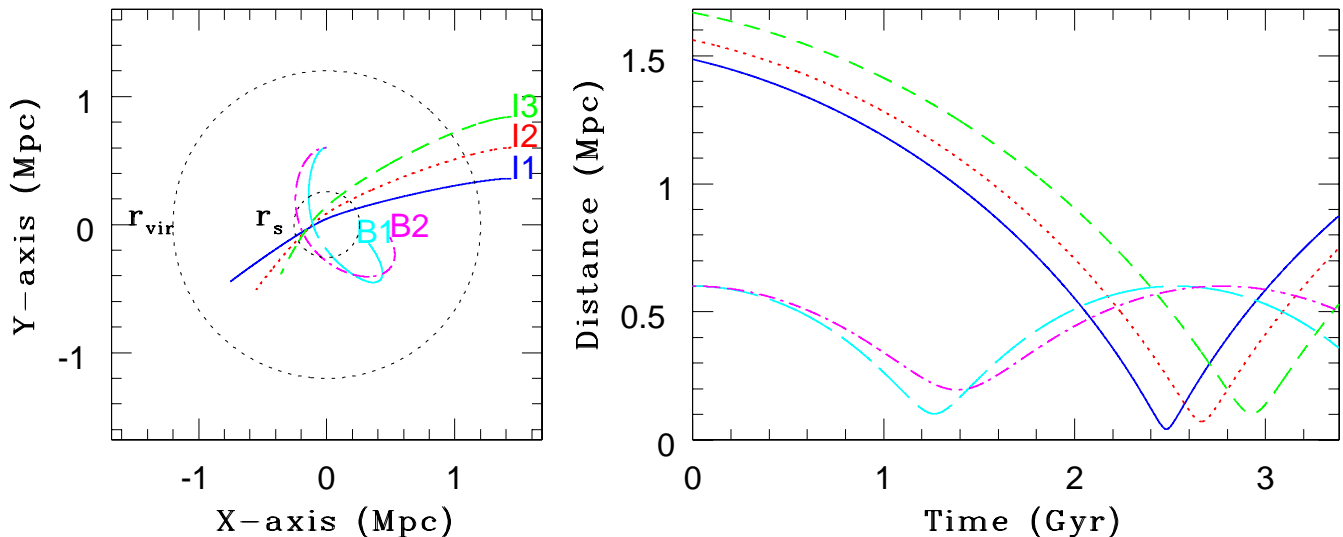


**Figure 1.** The orbit of a disk galaxy projected onto the  $x$ - $y$  plane (left) and the time evolution of the galaxy’s distance from the cluster center (right) for the five orbital types, I1 (blue, solid), I2 (red, dotted), I3 (green, short-dashed), B1 (cyan, long-dashed), and B2 (magenta, dot-dashed) in the low-mass Virgo cluster model. The inner and outer circles (black, dotted) indicate the scale radius ( $r_s$ ) and the virial radius ( $r_{\text{vir}}$ ) of the cluster, respectively.

models: Low-mass cluster model (‘Virgo’, labeled as ‘VI’) with  $M_h = 10^{14}M_\odot$  and  $T_{\text{ICM}} = 2.6 \times 10^7$  K and high-mass cluster model (‘Coma’, ‘CO’) with  $M_h = 10^{15}M_\odot$  and  $T_{\text{ICM}} = 1.2 \times 10^8$  K. These adopted  $T_{\text{ICM}}$  values are consistent with  $T_{\text{ICM}}$  estimated by X-ray observations for clusters with the above adopted masses (e.g., Matsumoto et al. 2000).

We also investigate massive group models with  $M_h = 10^{13}M_\odot$  and  $T_{\text{ICM}} = 5.6 \times 10^6$  K in order to investigate the influence of the halo gas of groups on SFHs of group member galaxies. These group models are referred to as ‘Group’ (‘GR’). The presence of intragroup gas and the influences of the gas on the evolution of group galaxy evolution have been observationally confirmed by previous X-ray observational studies for groups (e.g. Ponman et al. 1996; Helsdon & Ponman 2003; Rasmussen & Ponman 2007). It is therefore worthwhile for the present study to investigate the influences of ram pressure on galaxy evolution in groups. The initial total mass of ICM ( $M_{\text{ICM}}$ ) in a cluster/group is assumed to be  $0.15M_h$  in all models. The adopted value could be large for groups with smaller masses, because it is unlikely that most intragroup gas is in the form of hot gas. Furthermore, the radial density profiles of hot gas in the central regions of groups would significantly deviate from those of dark matter. This means that the present simulation could overestimate the effects of ram pressure of ICM on galaxies at pericenter passage for groups. The basic parameters for these three models are given in Table 2.

### 2.3.2 Galaxy orbits within clusters

A cluster of galaxies is assumed to have the NFW density profile and the  $c$ -parameter and  $r_{\text{vir}}$  are determined by  $M_h$

by using the formula by Neto et al. (2007). The orbit of a disk galaxy is determined by the adopted density profile of the cluster and the initial orbital plane is set to be the same as the  $x$ - $y$  plane in the cluster. The initial 3D position and velocity of the galaxy are denoted as  $(P_{x,0}, P_{y,0}, P_{z,0})$  and  $(V_x,0, V_y,0, V_z,0)$ , respectively. The density of ICM surrounding the galaxy at each time step is simply the dark matter density at the galaxy position multiplied by 0.15 (i.e., ICM mass fraction). Using the 3D velocity components of the galaxy at each time step,  $V_t(t)$  can be easily calculated.

We mainly investigate three ‘infall’ models (I1, I2, and I3) and two ‘bound’ ones (B1 and B2) for the orbital evolution of disk galaxies in clusters. For the infall models,  $P_{x,0} = 1.2r_{\text{vir}}$ ,  $P_{y,0} = f_x r_{\text{vir}}$  (where  $f_x$  is a parameter that corresponds to an impact parameter and thus controls the pericenter distance),  $P_{z,0} = 0$ ,  $V_{x,0} = -f_v v_c$  (where  $v_c$  is the circular velocity at the initial galaxy position and  $f_v$  is fixed at 0.3),  $V_{y,0} = 0$ , and  $V_{z,0} = 0$ . Accordingly, a galaxy can infall onto a cluster environment from outside the cluster virial radius and then pass through the cluster core. The smaller  $f_x$  is, the smaller the orbital pericenter distance is in these infall models. The  $f_x$  values are 0.3, 0.5, and 0.7 for I1, I2, and I3 models, respectively.

For the bound models,  $P_{x,0} = 0$ ,  $P_{y,0} = f_x r_{\text{vir}}$ ,  $P_{z,0} = 0$ ,  $V_{x,0} = -f_v v_c$ ,  $V_{y,0} = 0$  and  $V_{z,0} = 0$ . The models with smaller  $f_v$  show more eccentric orbits within a cluster for a given  $f_x$ . We mainly show the results of the models with  $f_x = 0.5$  and  $f_v = 0.3$  (B1) and  $f_v = 0.5$  (B2) in the present study. The initial 3D positions and velocities for the five models are given in Table 3. The orbital evolution of the five models (I1, I2, I3, B1, and B2) within a cluster with  $M_h = 10^{14}M_\odot$  is shown in Fig. 1.

**Table 3.** Description of the basic parameter values for the five orbital models.

Orbit type/Physical properties	I1	I2	I3	B1	B2
Initial position ( $P_{x,0}, P_{y,0}, P_{z,0}$ )	( $1.2r_{\text{vir}}, 0.3r_{\text{vir}}, 0$ )	( $1.2r_{\text{vir}}, 0.5r_{\text{vir}}, 0$ )	( $1.2r_{\text{vir}}, 0.7r_{\text{vir}}, 0$ )	( $0, 0.5r_{\text{vir}}, 0$ )	( $0, 0.5r_{\text{vir}}, 0$ )
Initial velocity ( $V_{x,0}, V_{y,0}, V_{z,0}$ )	( $-0.3v_c, 0, 0$ )	( $-0.3v_c, 0, 0$ )	( $-0.3v_c, 0, 0$ )	( $0, -0.3v_c, 0$ )	( $0, -0.5v_c, 0$ )

### 2.3.3 Disk inclination

The inclination angle of a disk with respect to the direction of the orbit in a cluster can be a key parameter that controls the total amount of gas stripped from the disk and thus the SFH. Since the orbital plane of a disk is the same as the  $x$ - $y$  plane, the spin axis of a disk with respect to the  $x$ - $y$  plane is a key parameter in the present study. The spin of the disk galaxy is specified by two angles  $\theta$  and  $\phi$  (in units of degrees), where  $\theta$  is the angle between the  $z$ -axis and the vector of the angular momentum of the disk, and  $\phi$  is the azimuthal angle measured from  $x$  axis to the projection of the angular momentum vector of the disk onto the  $x$ - $y$  plane. We mainly investigate the following three models: ‘face-on’ (labeled as ‘FA’) with  $\theta = 90$  and  $\phi = 0$ , ‘edge-on’ (‘ED’) with  $\theta = 0$  and  $\phi = 0$ , and ‘inclined’ (‘IN’) with  $\theta = 45$  and  $\phi = 30$ . In the face-on inclination model, a disk can be more strongly influenced by ram pressure stripping.

## 2.4 Parameter study

We mainly investigate the SFHs and 2D distributions of SF regions in MW-type, M33-type, and Dwarf-type disk galaxies for low-mass (Virgo) and high-mass (Coma) cluster models. For comparison, we also run an ‘isolated model’ in which ram pressure is not included at all. Since gas infall onto disks is not included in this isolated model, star formation can gradually decline in this model (i.e., this model does not correspond to field disk galaxy populations for which continuous gas infall might be possible for fueling SF).

We first show the results of the ‘fiducial’ model and then describe the parameter dependences of the present numerical simulations. In the fiducial model, the MW-type disk (‘MW’), the Virgo cluster model (‘VI’), face-on inclination (‘FA’), and I1 orbit (‘I1’) are adopted. The key parameters for the fiducial model are given in Table 4. This fiducial model is also labeled as ‘VI-I1-MW-FA’ and each model in the present study is labeled like this. For example, ‘CO-B1-DW-IN’ model means that a dwarf-type disk galaxy (‘DW’) with a gas disk inclined with respect to its orbital direction (‘IN’) is moving in a Coma-like cluster (‘CO’) with a highly eccentric bound orbit (‘B1’).

We mainly investigate SFHs and  $H\alpha$ -to-optical-disk-size ratio ( $s_{\text{sf}}$ ) in disk galaxies under strong ram pressure. We define  $s_{\text{sf}}$  as follows:

$$s_{\text{sf}} = \frac{R_{\text{sf}}}{R_{\text{s}}}, \quad (4)$$

where  $R_{\text{s}}$  is the size of the initial stellar disk composed only of old stars and  $R_{\text{sf}}$  is the size of the star-forming disk within which 98% of all new stars (with ages less than the lifetime of a  $8m_{\odot}$  star) are included. Although we could define  $R_{\text{sf}}$  as the distance of the most distant new star from its host galaxy’s center, we do not define  $s_{\text{sf}}$  as such. This is mainly because  $s_{\text{sf}}$  can change dramatically even within consecutive two time steps for data output, if  $R_{\text{sf}}$  is the distance of the most distant new star from the galaxy center. Therefore,

**Table 4.** Description of the basic parameter values for the fiducial model.

Physical properties	Adopted values
Cluster model	Low-mass (Virgo, $M_{\text{h}} = 10^{14}M_{\odot}$ )
Galaxy-type	MW ( $M_{\text{d}} = 5.4 \times 10^{10}M_{\odot}$ )
Orbit	I1
Disk inclination	( $\theta, \phi$ )=( $90^{\circ}, 0^{\circ}$ )

the number of 98% has no physical meaning and  $s_{\text{sf}}$  is used just for roughly estimating the size of the simulated  $H\alpha$  disk in a model and comparing it with the observed  $H\alpha$  disk. The half-mass radius of new stars in a simulated disk ( $R_{\text{h},\text{sf}}$ ), which could be more physically meaningful, is also investigated. This  $R_{\text{h},\text{ns}}$ , however, does not change so much in comparison with  $R_{\text{sf}}$  in the present models.

We also investigate 2D densities of SFRs and  $H\alpha$  by using the following formula (Kennicutt 1998);

$$\text{SFR}(M_{\odot}\text{yr}^{-1}) = \frac{L(H\alpha)}{1.26 \times 10^{41}\text{ergs}^{-1}}. \quad (5)$$

First we divide the simulated disk into  $50 \times 50$  cells and estimate the SFR density ( $\Sigma_{\text{SFR}} [M_{\odot} \text{yr}^{-1} \text{kpc}^{-2}]$ ) for each cell. Then  $H\alpha$  luminosity density for each cell can be estimated by using the above formula and  $\Sigma_{\text{SFR}}$ .

As previous numerical studies suggested (e.g., Kronberger et al. 2008; Bekki et al. 2010), high pressure of ICM can have positive (SF enhancement) and negative (SF reduction) effects on SFHs of disk galaxies in clusters. In order to understand which of the two effects can be more dominant for each model, we investigate the ratio of the total mass of new stars formed in a disk under ram pressure ( $M_{\text{ns}}$ ) to that in an isolated disk ( $M_{\text{ns},0}$ ). The ratio is accordingly represented by  $\epsilon_{\text{sf}}$  as follows:

$$\epsilon_{\text{sf}} = \frac{M_{\text{ns}}}{M_{\text{ns},0}}. \quad (6)$$

If this  $\epsilon_{\text{sf}}$  is larger than 1 in a model, it means that gas is more efficiently converted into new stars during 3.4 Gyr evolution of the disk within a group/cluster in comparison with the isolated model (i.e., ram pressure can enhance the conversion of cold gas into new stars). It should be noted here that the isolated model does not correspond to field galaxies (for which gas might continue to be accreted onto the gas disks so that SFRs can be kept constantly high, unlike the isolated model of the present study). Therefore,  $\epsilon > 1$  in a model does not mean that global SF in the disk is enhanced by ram pressure in comparison with field galaxies.

## 3 RESULTS

### 3.1 The fiducial model

Fig. 2 shows how the 2D distributions of cold gas and SFR in a MW-type disk galaxy changes with time when the galaxy passes through the central core of a Virgo-like cluster. In the early phase of its orbital evolution within the low-mass

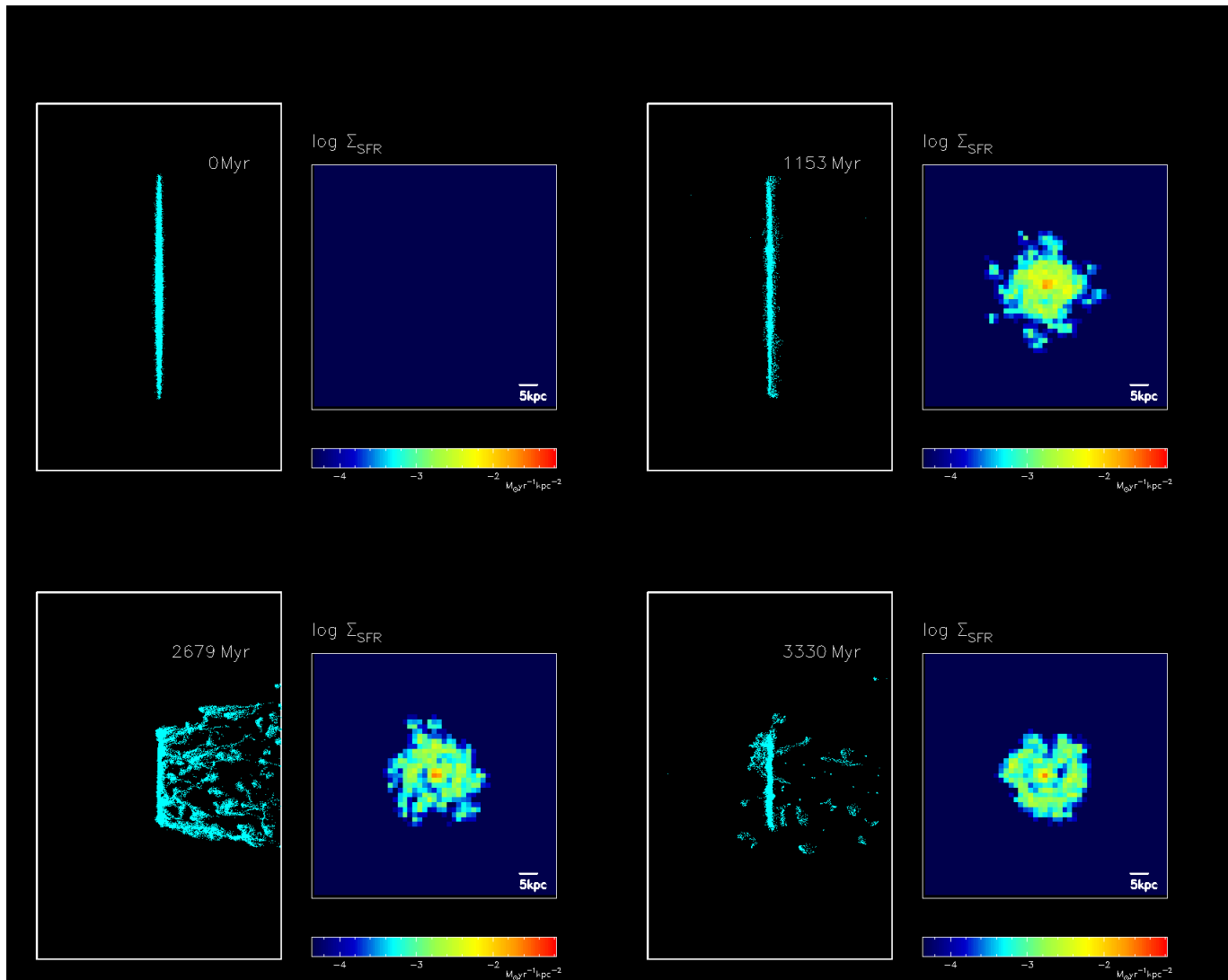


**Figure 2.** The gas distribution (edge-on view) of the disk galaxy (left, rectangular box) and the 2D distribution for the SFR density of young stars (right, square box) for the fiducial model with the MW-type disk, the Virgo cluster model, I1 orbit, and face-on disk inclination (labeled as ‘VI-I1-MW-IN’) at four different time steps. The rectangular panel for the projected gas distribution shows the time in units of Myr at the upper right corner. The 2D SFR density ( $\Sigma_{\text{SFR}}$  in logarithmic scale) is given in units of  $M_{\odot} \text{ yr}^{-1} \text{ kpc}^{-2}$ , and the thick bar in the lower right corner shows a physical scale of 5 kpc.

cluster, the ram pressure of ICM is rather weak and therefore can influence only the very outer part of the gas disk ( $T = 1.2$  Gyr). Consequently, new stars can continue to form throughout the gas disk as efficiently as the isolated disk in this early evolution phase. After the pericenter passage ( $r_p = 42$  kpc at  $T = 2.5$  Gyr), the gas disk can be quickly and efficiently stripped by ram pressure so that numerous small gas clumps can form behind the disk ( $T = 2.7$  Gyr). These small clumps have head-tail structures and most of them can be completely stripped from the disk galaxy (i.e., outside  $r_{\text{vir}}$ ) during the pericenter passage. However, a minor fraction of once stripped gas clumps can be returned back to the gas disk when the galaxy goes away from the orbital pericenter, because ram pressure can become weak again ( $T = 3.3$  Gyr). These clumps falling back to the original gas disk can be observed as high-velocity clouds in the galaxy.

The details of these stripping processes can be seen in the attached animation, for which the color codes are exactly the same as those in Fig. 2. The attached animation (ram.fl.avi for high-resolution and ram.fl.mov for low-resolution) clearly shows (i) how the gas disk of the disk galaxy in the fiducial model is stripped by ram pressure of ICM and (ii) how the 2D distribution of the star-forming regions accordingly changes during the disk evolution. This animation enables readers to understand better the following points that are not clearly shown in Fig. 2: (i) the formation processes of numerous small gas clumps during ram pressure stripping, (ii) the formation head-tail structures of the clumps, (iii) the re-accretion process of the clumps, and (iv) the sudden truncation of SF in the outer disk during ram pressure stripping.

Owing to the severe truncation of the outer gas disk by ram pressure stripping, SF in the outer disk ( $R \sim R_s$ )

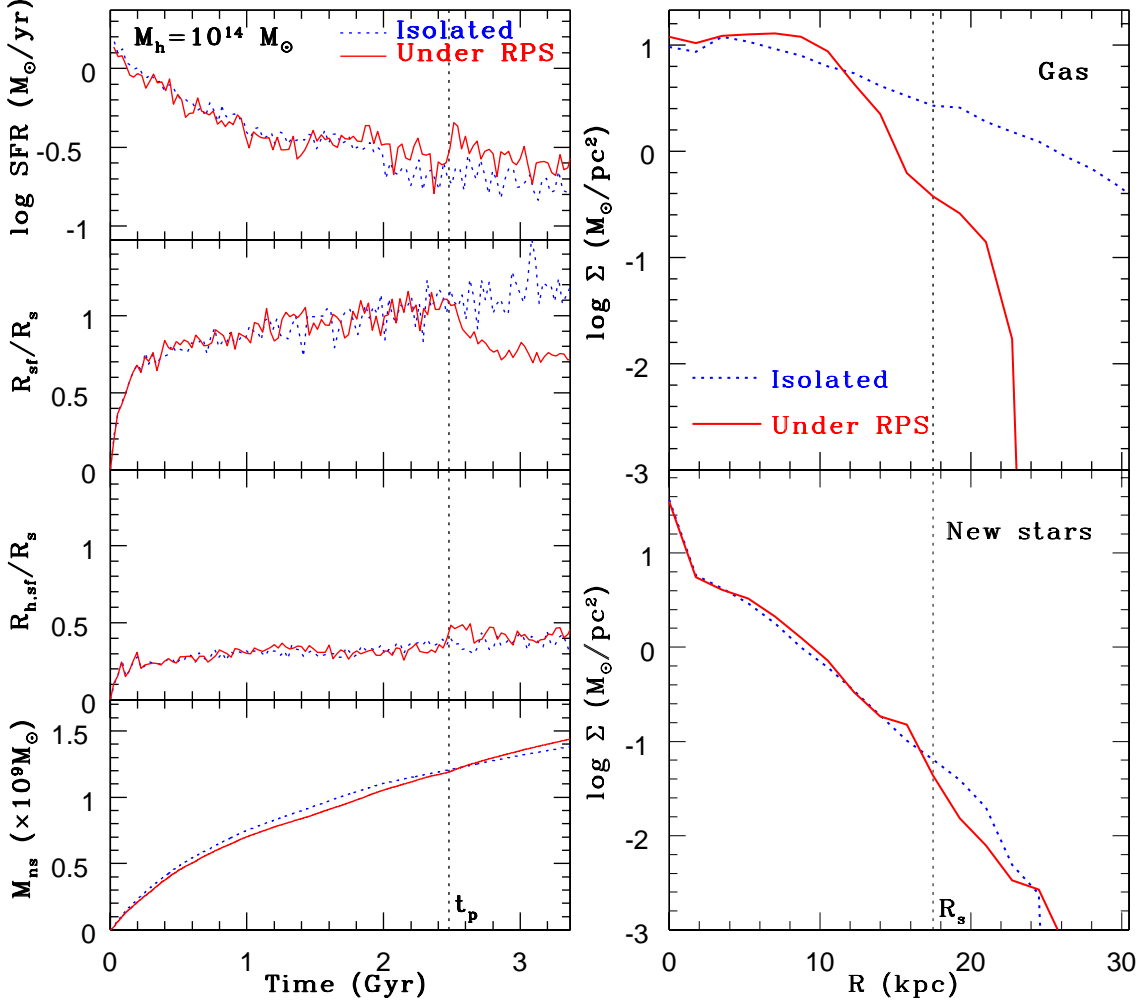


**Figure 3.** Left panel: The time evolution of star formation rate (SFR, top), the ratio of star-forming disk to initial stellar disk ( $R_{sf}/R_s$ , second from the top), the half-mass radius of new stars normalized by initial stellar disk size ( $R_{h,sf}/R_s$ , second from the bottom), and the total mass of new stars ( $M_{ns}$ , bottom) for the isolated model (blue, dotted) and the fiducial model under ram pressure stripping (labeled as ‘RPS’) within the Virgo-like cluster with  $M_h = 10^{14} M_{\odot}$  (red, solid). The black dotted line indicates the time of pericenter passage ( $t_p$ ). Right panel: The final projected distributions of gas (upper) and new stars (lower) for the isolated model (blue, dotted) and for the fiducial model (red, solid).

can be completely shut down. As a result of this, the 2D  $\Sigma_{\text{SFR}}$  distribution shows a sharp edge around  $R \sim 12$  kpc at  $T = 3.3$  Gyr. It is intriguing that the outer 2D  $\Sigma_{\text{SFR}}$  distribution looks like a ring with a central concentration. This ring-like distribution of new stars is characteristic for disk galaxies under strong ram pressure stripping, as discussed later. The left panel of Fig. 3 shows that in spite of efficient gas stripping, the SFR of the disk galaxy can become higher than the SFR of the isolated model at  $T > 2$  Gyr. A physical explanation for this moderate SF enhancement is as follows. When the disk galaxy becomes closer to the orbital pericenter, ram pressure becomes moderately strong and starts to compress the inner part of the gas disk so that a significant fraction of gas particles can have higher gas densities. This compression of gas by ram pressure can be the strongest at the pericenter passage of the galaxy. As a result of this, SF can be moderately enhanced largely in the central region of the disk at the pericenter passage. The physical mechanism of this is discussed more extensively in §3.5.

The left panel of Fig. 3 shows that  $s_{sf}$  ( $= R_{sf}/R_s$  corresponding to the observed H $\alpha$ -to-optical-disk-size ratio) can become significantly smaller after the pericenter passage owing to the truncated SF in the outer disk. The half-mass radius of new stars ( $R_{h,ns}$ ), however, does not change significantly during ram pressure stripping. This means that ram pressure can only influence the outer star-forming disk in this model. The total mass of new stars ( $M_{ns}$ ) formed during  $\sim 3.4$  Gyr evolution of the disk is only slightly larger than that in the isolated model, which means that the positive effect of ram pressure on SF (i.e., SF enhancement) can surpass the negative one (i.e., SF reduction) in this MW-type disk galaxy. It should be noted, however, that it depends on  $M_h$ ,  $r_p$ , and  $\theta$  ( $\phi$ ) of disk galaxies on which of these two effects can be more dominant in SFHs of disk galaxies for a given environment (This point is later discussed in §3.2.)

The right two panels of Fig. 3 show that the final projected density distributions ( $\Sigma$ ) of gas are quite different between the isolated and fiducial models, though the distri-

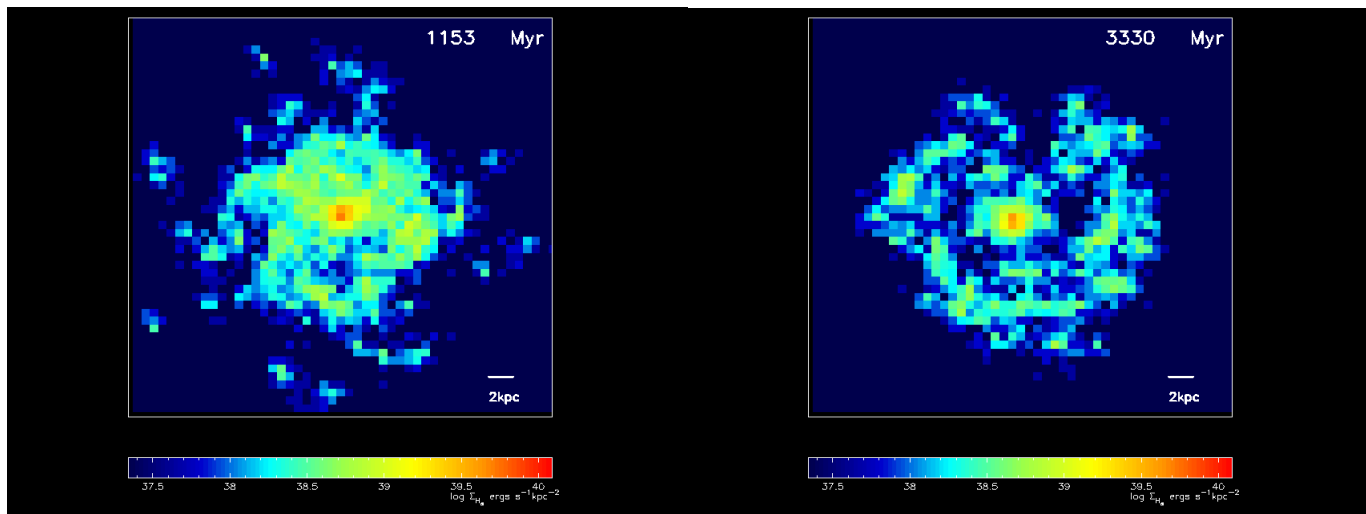


**Figure 4.** The 2D distributions of H $\alpha$  emission densities ( $\Sigma_{\text{H}\alpha}$ , in logarithmic scale) for the fiducial model at  $T = 1153$  Myr (left) and  $T = 3330$  Myr (right). These 2D H $\alpha$  maps are from 2D SFR density maps shown in Fig. 2. Clearly, the disk at  $T = 3330$  Myr (i.e., after ram pressure stripping) shows an outer ring-like structure in the H $\alpha$  map.

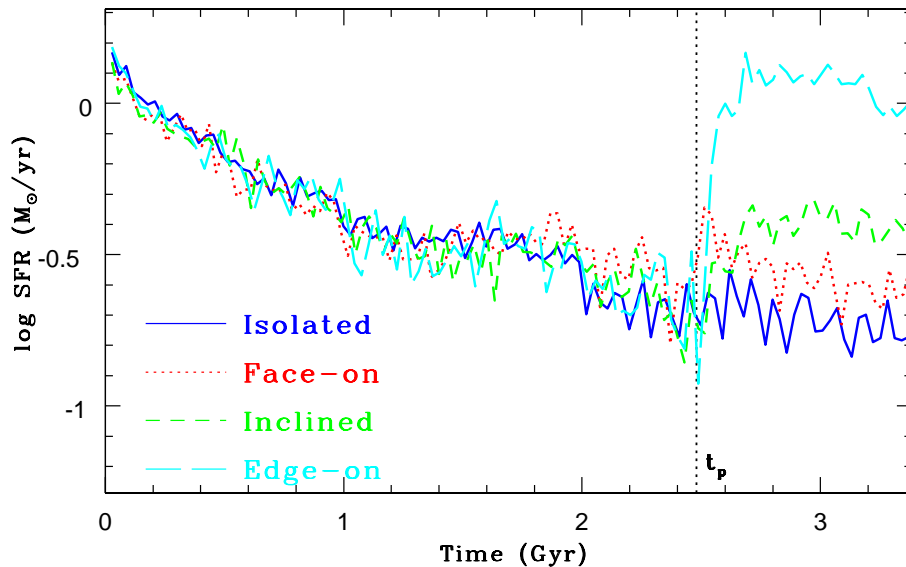


**Figure 5.** The time evolution of SFRs in the MW-type disk galaxies with Face-one (red, dotted), Inclined (green short-dashed), and Edge-on (cyan, long-dashed) disk orientation models within the low-mass Virgo cluster. For comparison, the isolated disk model is shown by a blue solid line. The time at the pericenter passage is indicated by a black dotted line and marked with ‘ $t_p$ ’. It is clear that the Edge-on model shows a greater enhancement of SF after pericenter passage owing to the stronger compression of ISM by ram pressure.

butions of new stars are not so different between the two. The gaseous distributions with almost constant  $\Sigma$  for  $4 \text{ kpc} \leq R \leq 10 \text{ kpc}$  and very steep  $\Sigma$  decline beyond  $R \sim 10 \text{ kpc}$  in the fiducial model clearly mean that ram pressure can significantly increase the gas density in the inner region of the gas disk. The inner region with constant  $\Sigma$  is roughly coincident with the location of a ring-like structure of young stars shown in Fig. 2 (and later in Fig. 4). This coincidence provides the following explanation for the origin of the ring-like structure. During efficient ram pressure stripping of the outer gas disk (which ends up with the sharp  $\Sigma$  decline at  $R > 10 \text{ kpc}$  in Fig.3), the inner gas disk can be strongly

compressed by ram pressure. Consequently, the gas density of the inner gas disk ( $4 \text{ kpc} \leq R \leq 10 \text{ kpc}$ ) can become so high that new stars can form from the gas disk. The gas at the circumnuclear region ( $R \sim 2 \text{ kpc}$ ) can be rapidly consumed by star formation so that the SFR there can be relatively low at the time of pericenter passage. Thus, a ring-like young star-forming region can be formed after ram pressure stripping.

The right panel of Fig. 4 shows that (i) SF can be actively ongoing in the central bulge region and (ii) the disk has an intriguing ring-like H $\alpha$  morphology after ram pressure stripping of the outer gas disk ( $T = 3.3 \text{ Gyr}$ ). The outer

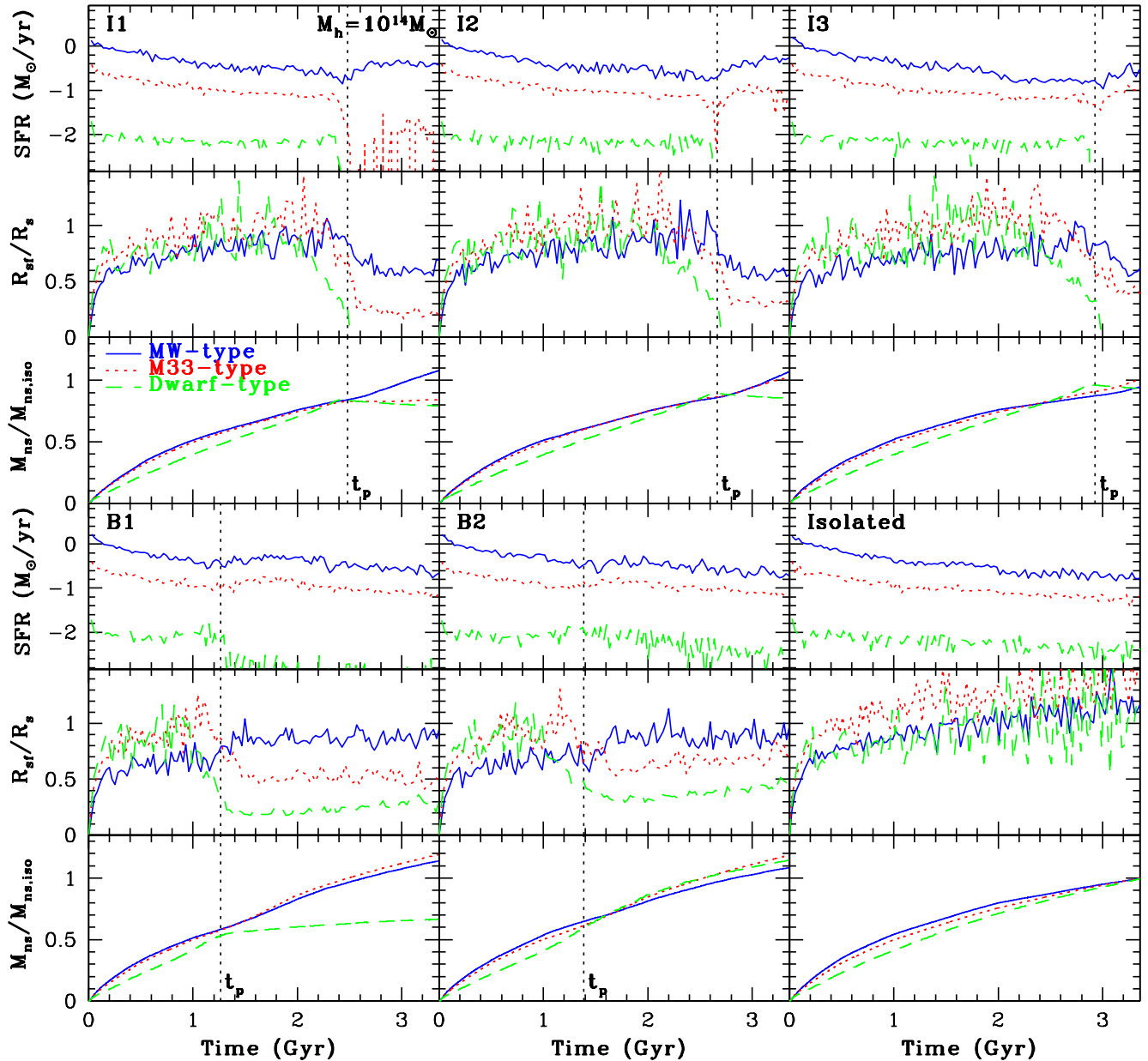


**Figure 6.** The time evolution of SFRs (in logarithmic scale),  $s_{\text{sf}} (= R_{\text{sf}}/R_s)$ , and  $\epsilon_{\text{sf}} (= M_{\text{ns}}/M_{\text{ns},0})$  for 15 different disk galaxies with different orbits and halo masses in the low-mass Virgo cluster model with  $M_h = 10^{14} M_\odot$ . Each of six sets of three frames shows the results of the three different disk galaxies, MW-type (blue, solid), M33-type (red, dotted), and Dwarf-type (green, dashed), with a specific orbital type (I1, I2, I3, B1, and B2, indicated in the upper left corner of the top panel). For comparison, the results of the three isolated models are also shown. The time of pericenter passage ( $t_p$ ) is shown by a vertical black dotted line in each panel.

sharp edge of the H $\alpha$  ring corresponds to the outer edge of the truncated gas disk. Given that such a ring-like structure can not be seen in the disk at  $T = 1.2$  Gyr (left panel of Fig. 4) and in the isolated model, the formation of the ring is caused by the effects of ram pressure on the gas disk. Such a ring-like distribution of star-forming regions is indeed observed for NGC 4569 in the Virgo cluster (e.g., Koopmann & Kenny 2004). The simulated ring-like H $\alpha$  morphology is one of characteristic distributions of H $\alpha$  in disk galaxies under strong ram pressure, as described later.

### 3.2 Parameter dependence

Figs. 5–8 summarize the dependences of the time evolution of SFRs,  $s_{\text{sf}}$  (corresponding to H $\alpha$ -to-optical-disk-size ratio), and  $\epsilon_{\text{sf}}$  (long-term conversion efficiencies of cold ISM into new stars) on disk inclination angles ( $\theta$  and  $\phi$ ), halo masses of galaxies ( $M_h$ ), orbits (e.g.,  $r_p$ ), and group/cluster masses ( $M_g$ ). For Figs. 5–7, the results of the disk models with  $\theta = 45^\circ$  and  $\phi = 30^\circ$  (‘IN’ models) are shown, because such inclined disk configurations with respect to the orbits

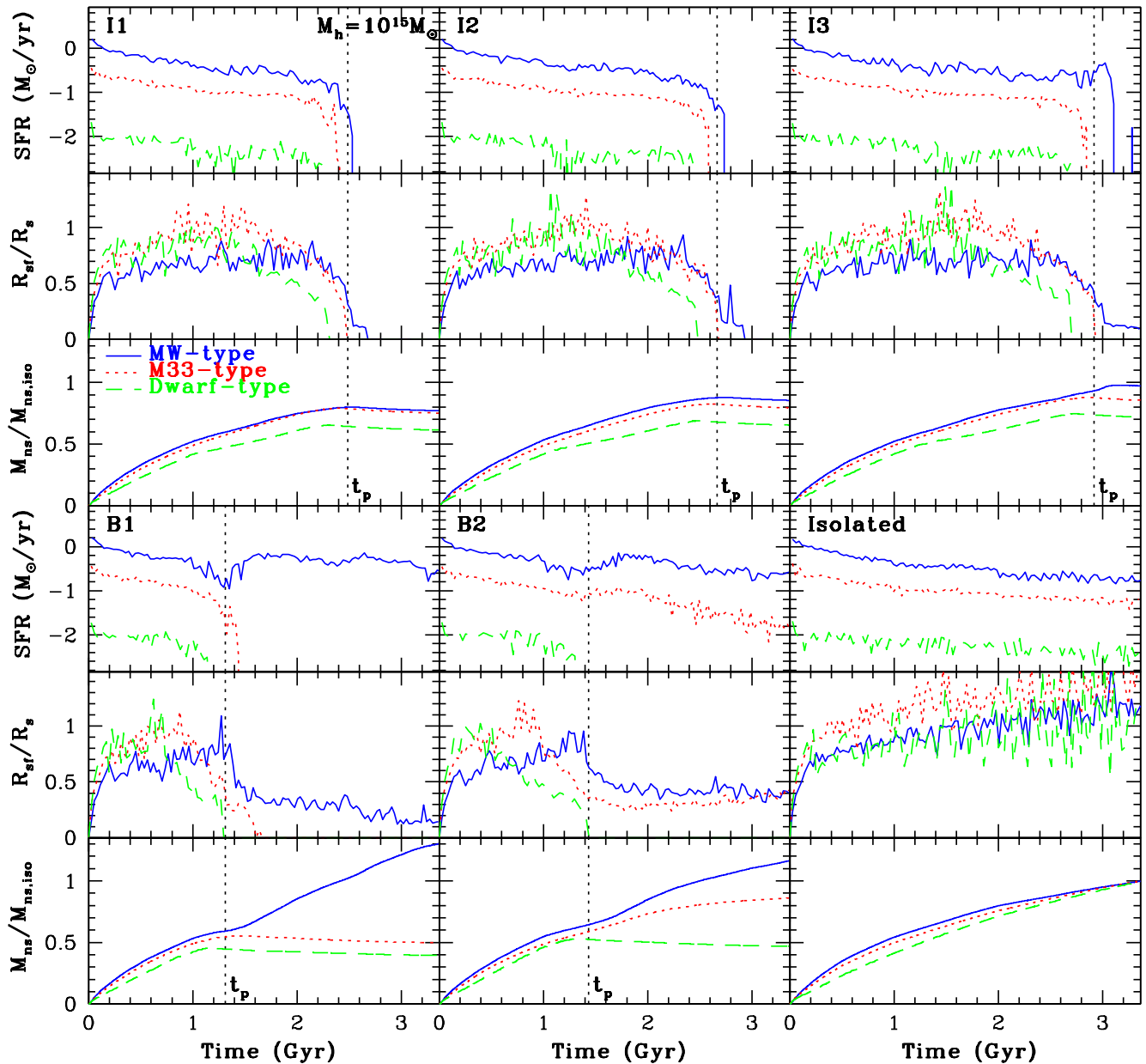


Figure 7. The same as Fig. 6 but for the Coma model with  $M_h = 10^{15} M_{\odot}$ .

of galaxies can be more typical and more realistic for real ISM-ICM interaction in groups and clusters.

### 3.2.1 Disk inclination

As shown in Fig. 5, SFHs of MW-type galaxies after pericenter passage depend strongly on disk inclination angles for the low-mass Virgo cluster model. Clearly, SF can be more strongly enhanced by ram pressure in the edge-on disk inclination than in the face-on and inclined ones. Ram pressure can be responsible both for efficient gas stripping and for strong compression of gas. For the edge-on model, the latter effect is more dominant than the former one so that SF can be significantly enhanced in the central region of the gas

disk. The level of SF enhancement in the edge-on model is significant (i.e., similar to the initial active SF phase) and can continue for  $\sim 1$  Gyr after pericenter passage. Either ‘reactivation’ or ‘rejuvenation’ would be a better word for describing the effect of ram pressure on the galactic SFH of the edge-one model.

### 3.2.2 Galaxy mass

As shown in Fig. 6, both SFRs and  $s_{\text{sf}}$  can be more significantly reduced in less massive disk galaxies for the I1 orbit in the Virgo cluster model with  $M_h = 10^{14} M_{\odot}$ . The MW-type galaxy shows a slightly enhanced SFR after pericenter passage whereas the M33-type shows a sudden and signif-

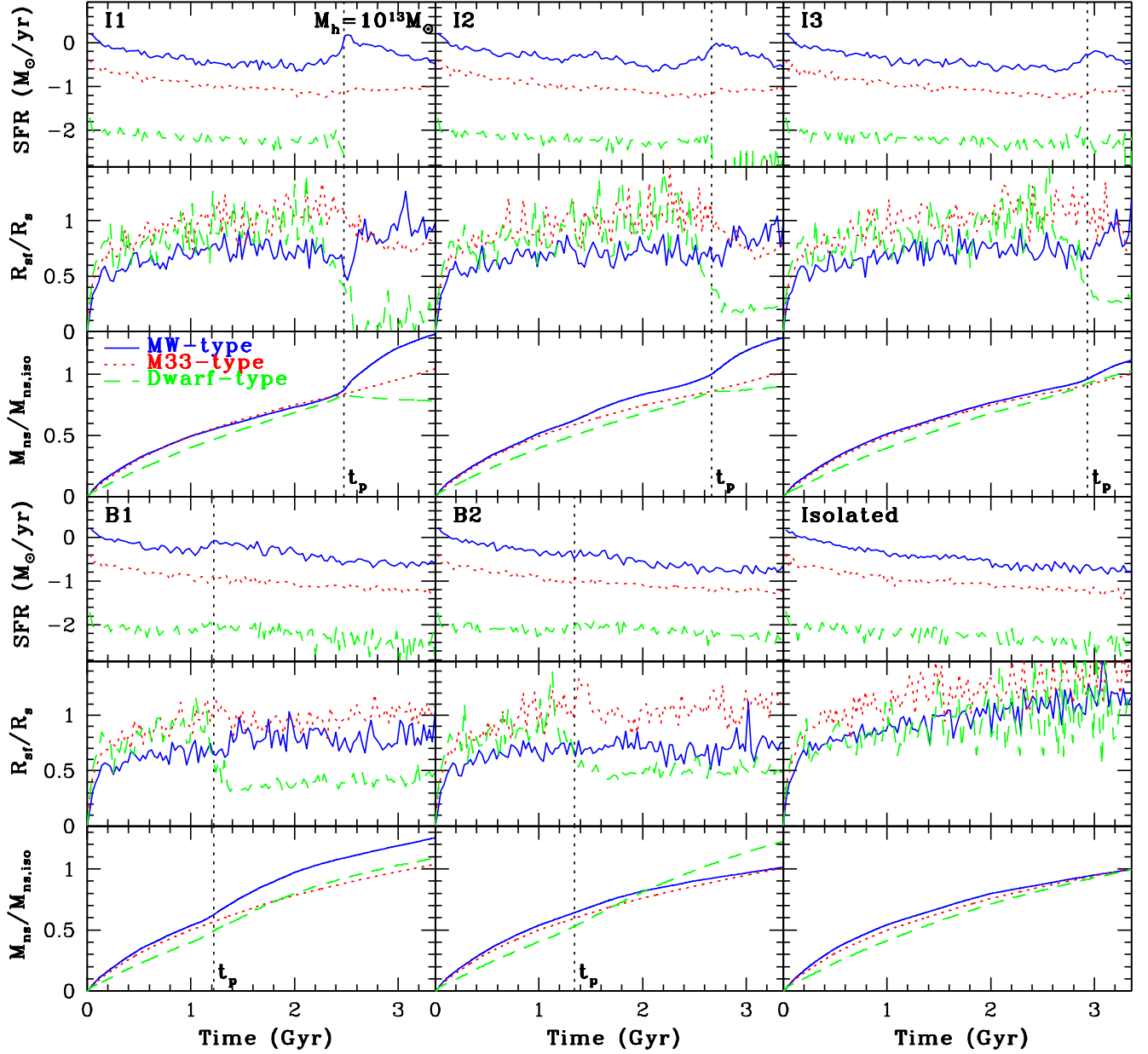
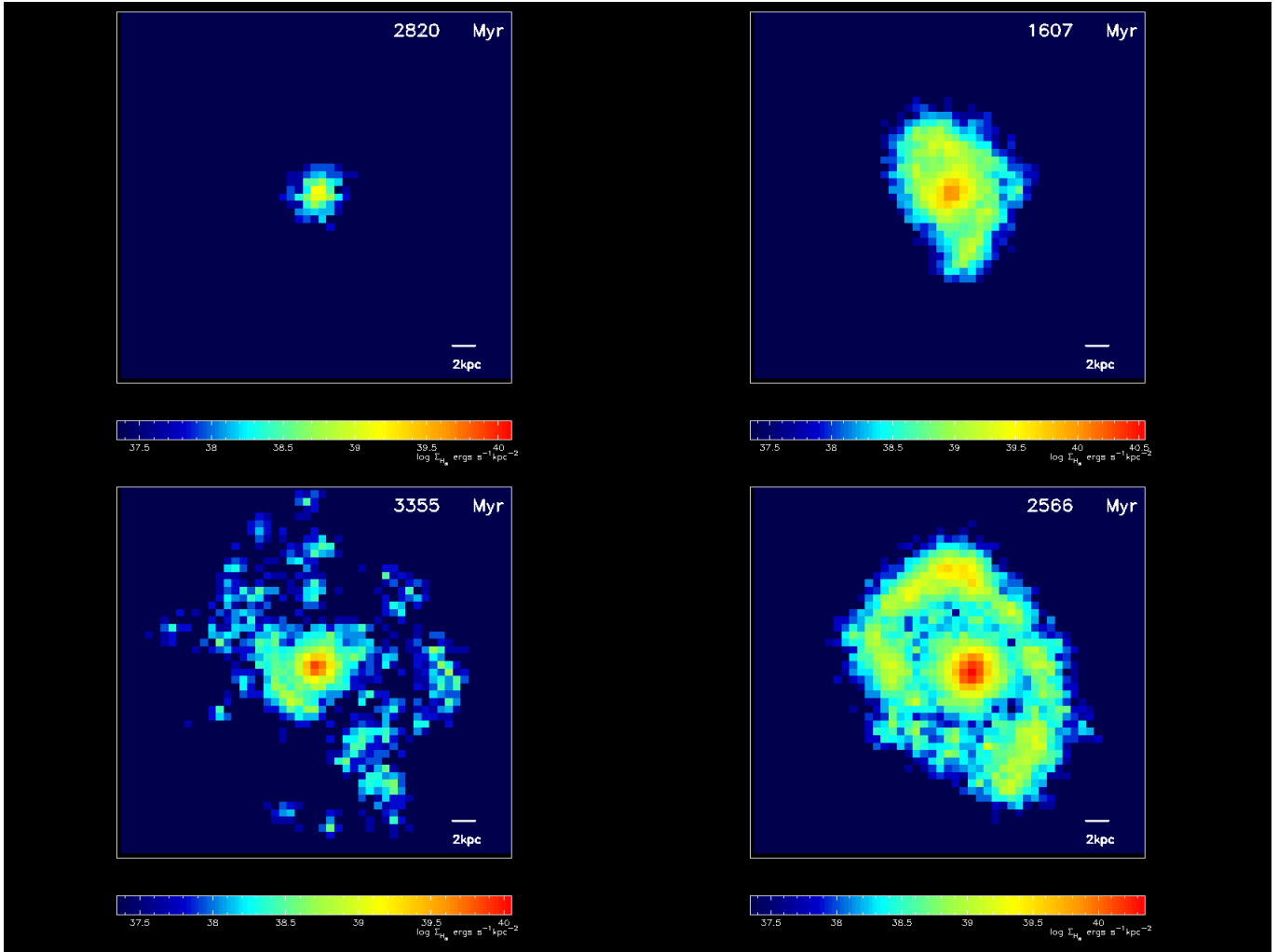


Figure 8. The same as Fig. 6 but for the Group model with  $M_h = 10^{13} M_\odot$ .

icant SFR decrease in the I1 orbit. The  $s_{sf}$  parameter can be reduced by  $\sim 40\%$  for the MW-type and by  $\sim 80\%$  for the M33-type in this orbit, which means that the M33-type has a more compact H $\alpha$  disk. SF in the Dwarf-type can be suddenly shut down (‘SF quenching’) and thus  $s_{sf}$  becomes 0 after pericenter-passage owing to the complete stripping of cold gas from the disk by ram pressure in this I1 orbit. The  $\epsilon_{sf}$  parameter can become larger than 1 for the MW-type owing to the moderate SF enhancement in the central bulge region whereas it can be significantly lower than 1 for M33-type and Dwarf-type in this I1 orbit. These results suggest that SFHs and 2D distributions of SF regions in less massive disk galaxies can be more strongly influenced by ram pressure in clusters.

The modest SF enhancement of the MW-type and the sudden SF quenching of the Dwarf-type derived in the I1 orbit can be seen in other orbits of the Virgo model and in some orbits of the Coma and the Group models. However, the significant SF reduction of the M33-type derived in the I1 orbit can not be clearly seen in other orbits of the Virgo models. This simply means that SFHs of disk galaxies can be determined not only by their masses but also by other parameters ( $r_p$  and group/cluster masses). The dependences of the time evolution of  $s_{sf}$  on galaxy masses derived in the I1 orbit of the Virgo model can be seen in other orbital types (I2, I3, B1, and B2) of the Virgo model and some orbits of the Coma cluster model (See Fig. 7). The degrees of SF and  $s_{sf}$  reduction by ram pressure, however, can depend on



**Figure 9.** A collection of four characteristic  $H\alpha$  morphologies in disk galaxies under ram pressure derived from four models, CO-I2-MW-IN (upper left), CO-B1-MW-IN (upper right), VI-B1-MW-IN (lower left), and GR-I1-MW-IN (lower right). These  $H\alpha$  maps show very compact and truncated (upper left), one-sided or crescent-like (upper right), outer (broken), ring-like (lower left), and outer high-density ring-like distributions (lower right). These four are chosen from many  $H\alpha$  distributions of models at different time steps.

orbital types and group/cluster masses, as shown in Figs. 6–8, which is described later. It should be noted that moderate SF enhancement by ram pressure can be clearly seen only in the MW type (not so clear in the M33-type and the Dwarf-type for all models).

### 3.2.3 Orbit

The orbital pericenter distances ( $r_p$ ) are 42, 72, 102, 102, and 195 kpc for the orbital types I1, I2, I3, B1, and B2 in the Virgo model. Accordingly, it is clear from Figs. 6 that  $s_{sf}$  can be more significantly reduced in the M33-type with smaller  $r_p$  among the three infall models (I1, I2, and I3). This dependence on  $r_p$  can be seen in the M33-type and the Dwarf-type for the two bound orbits. Although final  $s_{sf}$  for the MW-type is significantly smaller than that of the isolated model for all orbits, the dependence of final  $s_{sf}$  on  $r_p$  is not so clear for the MW-type. Smaller final  $\epsilon_{sf}$  and more significant SF reduction are likely to occur in the Dwarf-type with smaller  $r_p$ . These derived dependences of SFHs,

$s_{sf}$ , and  $\epsilon_{sf}$  can be seen in the Coma model and the Group one. These dependences on the orbits of galaxies are due largely to the differences of the influences of ram pressure force on gaseous evolution (thus on SFHs) between different models.

The differences in  $t_p$  (the epoch of pericenter passage) between models with different orbits can be as large as  $\sim 1$  Gyr. This means that the total gas masses ( $M_g$ ) of disks at  $t_p$  can be significantly different between different models thus that the restoring force of gas disks can be different between the models at  $t_p$ . Therefore the differences of  $M_g$  at  $t_p$  might be responsible for the dependences of the present results on the orbits of galaxies. However, the differences in  $M_g$  at  $t_p$  between models with different orbits are rather small. For example,  $M_g$  in the isolated MW model is  $1.11 \times 10^{10} M_\odot$  at  $t_p \sim 1.3$  Gyr (corresponding to the VI-B1-MW-IN model) and  $1.08 \times 10^{10} M_\odot$  at  $t_p \sim 2.4$  Gyr (VI-I1-MW-IN model). These values can be roughly estimated from the time evolution of  $M_{ns}$  in Fig. 3 and the adopted larger initial  $M_g$  ( $1.2 \times 10^{10} M_\odot$ ). Therefore, the

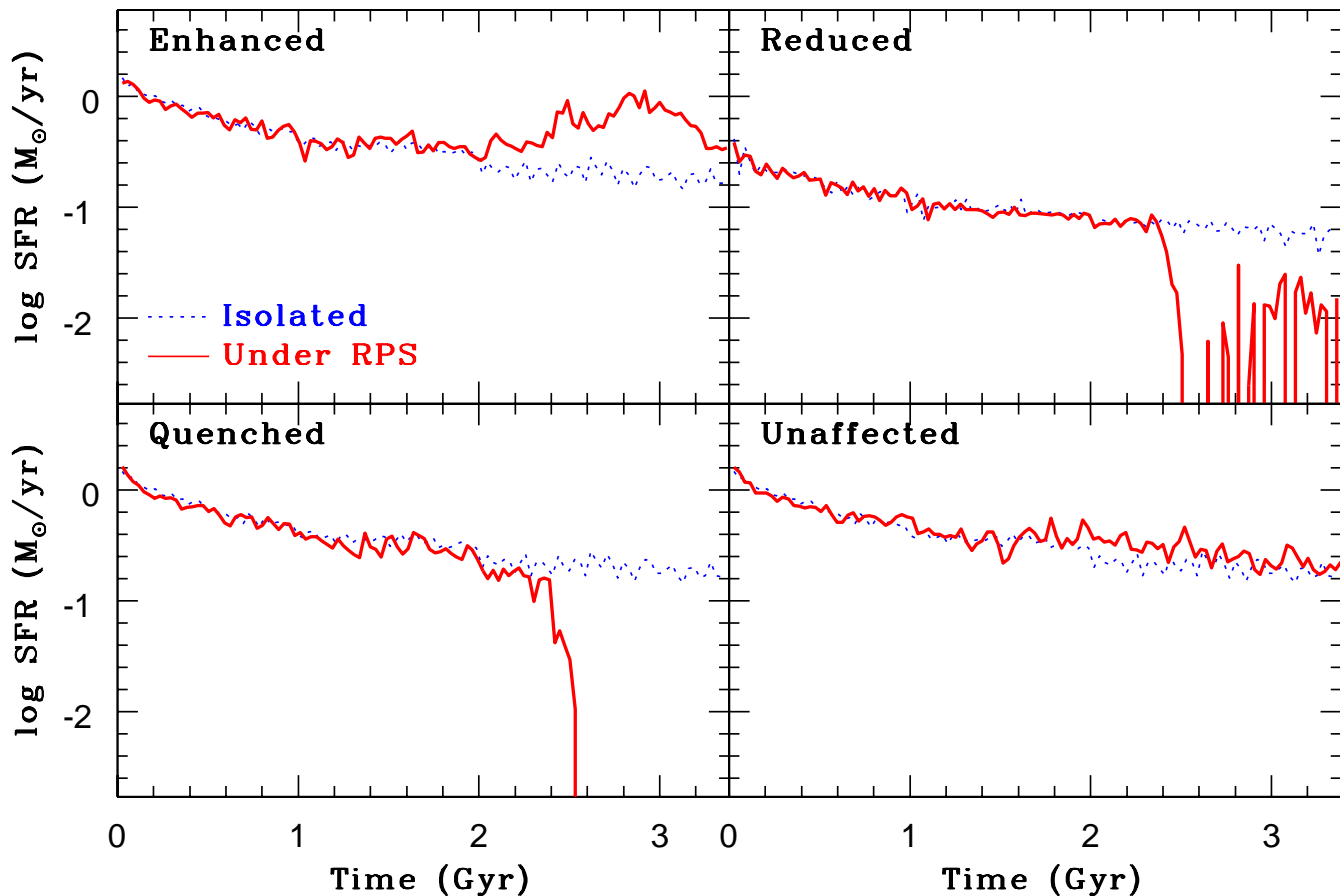


**Figure 10.** The time evolution of SFRs for four representative SF modes derived for disk galaxies under ram pressure (red, solid): Enhanced (upper left, the model CO-I2-MW-ED), Reduced (upper right, VI-I1-M33-IN), Quenched (lower left, CO-I1-MW-IN), and Unaffected (lower right, VI-B2-MW-IN). For comparison, the isolated model is shown by a blue dotted line in each panel. Ram pressure does not always reduce or quench galactic star formation, but it can enhance significantly depending on galaxy masses, inclination angles, pericenter distances, and groups/cluster masses. The ‘Unaffected’ SF mode means that SF of galaxies are much less influenced by ram pressure: It does not mean that SF is not influenced by ram pressure at all (very slight increase of SF can be seen in the model shown in the lower right panel).

possible small difference ( $\sim 3\%$ ) in the restoring force of gas disks is highly unlikely to influence the time evolution of SF in disks under ram pressure. We therefore consider that the derived dependences of the present results on the orbits of galaxies are due largely to the differences of the influences of ram pressure force on gas disks between different models.

### 3.2.4 Group/cluster mass

Fig. 7 shows that irrespective of galaxy-masses, SF in disks can be suddenly and completely truncated after pericenter passage in the Coma model, as long as  $r_p$  is small enough. Not only the M33-type and the Dwarf-type but also the MW-type shows SF quenching in the orbit I1 and I2 in this massive cluster model. These results are in a striking contrast with those for the low-mass Virgo model, which implies that SF in MW-type disk galaxies can be quenched only in massive clusters. It is intriguing that SF enhancement does not occur for the MW-type in I1 and I2 of the Coma model, though SF enhancement can be frequently seen in the Virgo

model and the Group one. This result implies that moderately strong ram pressure is required for SF of MW-type disk galaxies to be moderately enhanced. Too strong ram pressure can simply strip the entire gas disk so that SF enhancement by compression of gas by ram pressure can not occur.

Fig. 8 shows that SF enhancement by ram pressure after pericenter passage in the MW-type is more pronounced in the Group model than in the Virgo one (in particular, orbits I1 and I2). Furthermore, the final  $\epsilon_{sf}$  in the MW-type is significantly larger than 1 for these I1 and I2 orbits, which means that cold gas is more efficiently converted into new stars owing to compression of gas by ram pressure. These results imply that although  $s_{sf}$  of luminous disk galaxies in a group can become slightly smaller (i.e., slightly truncated  $H\alpha$  disk) owing to ram pressure of the intragroup gas, their SF activity can be enhanced, as long as their  $r_p$  can be small enough. The Dwarf-type with smaller  $r_p$  (I1 and I2 orbits) shows almost complete truncation of SF even in this group environment. It should be noted, however, that the DW-type

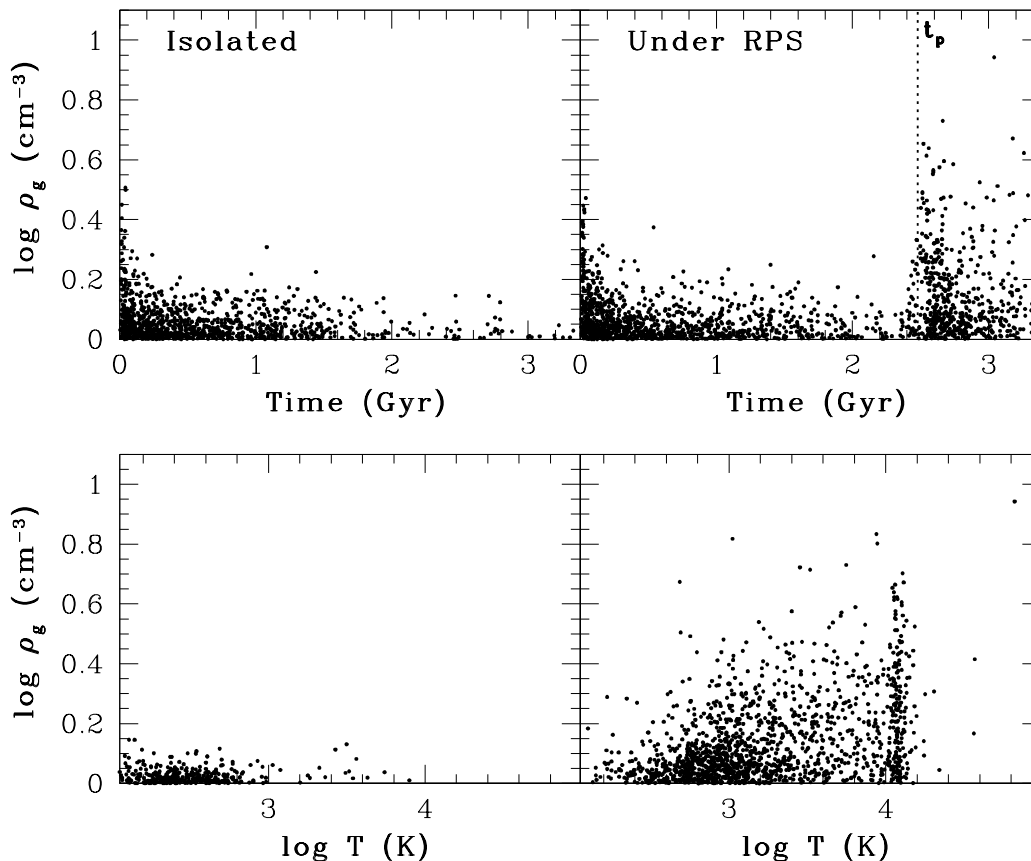


**Figure 11.** Upper panel: The time evolution of gas densities ( $\rho_g$  in units of H-atom number per  $\text{cm}^3$ ) for the isolated model and the model (VI-I1-MW-ED) under ram pressure stripping (right). The star formation histories of these models are already shown in Fig. 5. These gas particles are those which are converted into new stars. The file size of this figure can be very large ( $\sim 7$  MB), if all gas particles are plotted. Therefore, one every 20 particles is plotted in the upper panel so that the file size can be much smaller. Nevertheless the differences in the time evolution of  $\rho_g$  between the two models can be still clearly seen in the upper panel. Lower panel: The locations of gas particles on the density-temperature ( $\rho_g - T$ ) plane for the isolated model (left) and the VI-I1-MW-ED model (right). The gas particles that are converted into new stars only after pericenter passage (2.48 Gyr) are shown (for the two models) so that the influences of ram pressure on the distributions of (star-forming) gas on the  $\rho_g - T$  plane can be more clearly understood. One every 10 particles is plotted in this lower panel.

with the B2 orbit shows a very slight SF enhancement after pericenter passage (in comparison with the isolated model) and thus  $\epsilon_{\text{sf}} > 1$ . These results suggest that ram pressure of intragroup gas can be important for the SFHs of disk galaxies in group environments.

### 3.3 Characteristic H $\alpha$ morphologies

Fig. 9 presents a collection of the following four characteristic H $\alpha$  morphologies seen in the simulated disk galaxies of the present study: (i) very compact and severely truncated, (ii) one-sided and outer crescent-like, (iii) broken ring-like and patchy, and (iv) an outer high-density ring (distributions). These characteristic H $\alpha$  morphologies are not seen in isolated models and thus regarded as being due to ram pressure effects. The severely truncated distribution can be seen more frequently in disk galaxy models just before the complete truncation of SF by ram pressure. The one-sided or crescent-like (or one-spiral-arm-like) distribution can be more clearly seen in disk galaxy models with edge-on disk inclination in which only one side of the gas disk can be

strongly influenced by hydrodynamical force of ram pressure. Disk galaxies with these crescent-like H $\alpha$  distributions often show enhanced global SFRs.

The broken ring-like distributions can be frequently seen in disk models with face-on ( $\theta = 90^\circ$  and  $\phi = 0^\circ$ ) or inclined ( $\theta = 45^\circ$  and  $\phi = 30^\circ$ ) disk configurations. This ring-like distribution is not due to the dynamical action of central bars, because it is confirmed that this ring-like distribution can be seen in the disk models with big bulges for which bar formation via global bar instability is unlikely. The outer rings with significant SF enhancement within the rings can be seen for disk galaxy models with smaller  $r_p$  orbiting the Group. The ring-like distributions of enhanced SF regions can not be seen in isolated models, which suggests that such ring-like distributions can be used for searching for evidence of an environmental effect of a group on SFHs of disk galaxies.

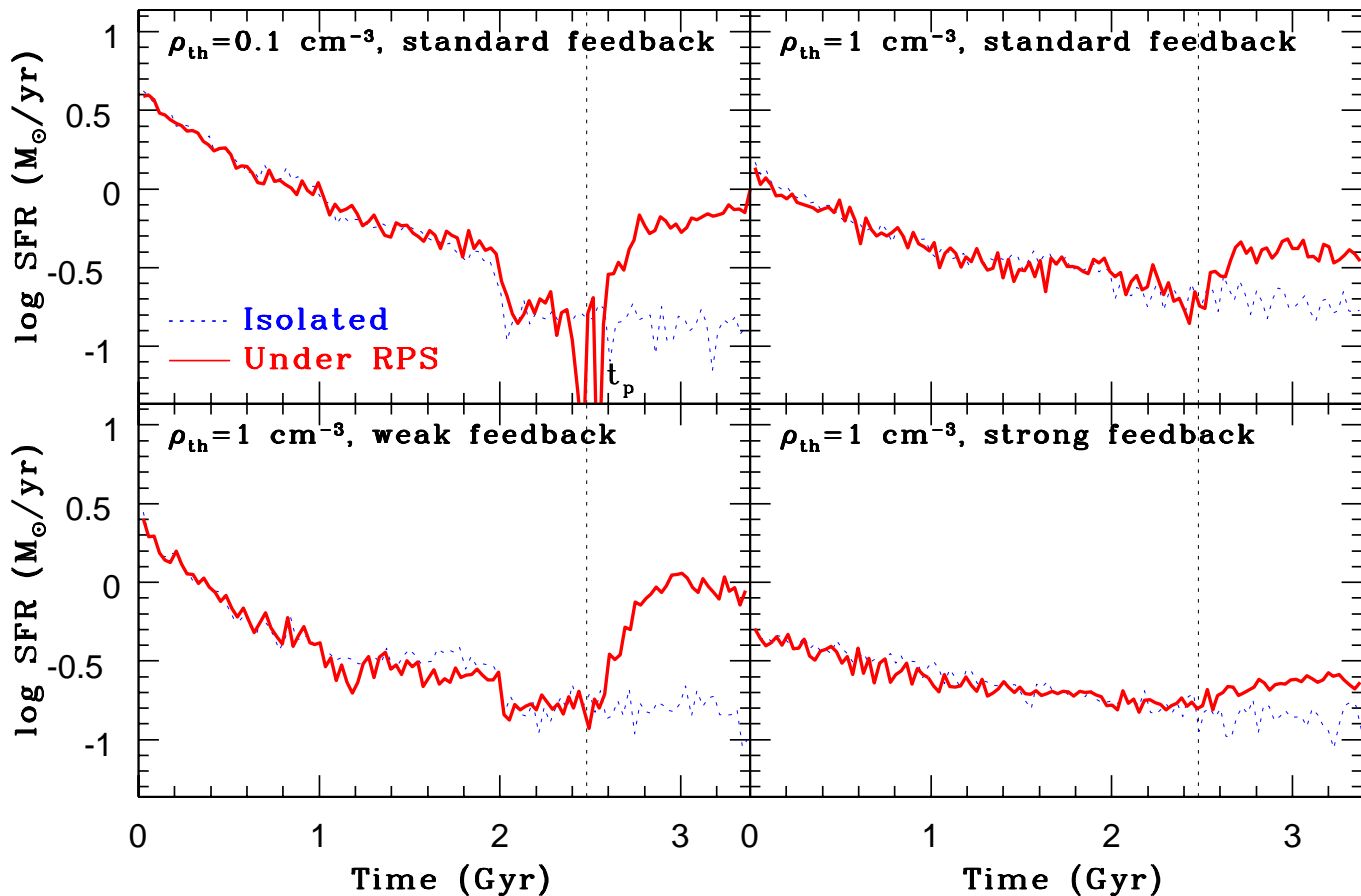


**Figure 12.** The time evolution of SFRs for models with  $\rho_{\text{th}} = 0.1 \text{ cm}^{-3}$  and standard SN feedback (upper left), with  $\rho_{\text{th}} = 1 \text{ cm}^{-3}$  and standard SN feedback (upper right), with  $\rho_{\text{th}} = 1 \text{ cm}^{-3}$  and weak SN feedback effect (lower left), and with  $\rho_{\text{th}} = 1 \text{ cm}^{-3}$  and strong SN feedback effect (lower right). Here weak, standard, and strong SN feedback models assume  $t_{\text{adi}} = 3 \times 10^5 \text{ yr}$ ,  $10^6 \text{ yr}$ , and  $10^7 \text{ yr}$ , respectively. The black dotted line indicates the time of pericenter passage ( $t_p$ ). The isolated model and the model under ram pressure stripping are shown by blue dotted and red solid lines, respectively, in each frame.

### 3.4 Four modes of SF

Fig. 10 summarizes the following four basic modes of SF in disk galaxies orbiting groups and clusters of galaxies: (i) Enhanced, (ii) Reduced, (iii) Quenched, and (iv) Unaffected (SF). The ‘Enhanced SF’ mode means that SFRs can be moderately enhanced by ram pressure but can not be as high as the SFRs of starburst galaxies whereas the ‘unaffected SF’ mode means that SFRs can not change significantly (though very slight increase in SF can be seen during/after ram pressure). The Enhanced SF mode is more frequently seen in the MW-type whereas the Quenched and Reduced SF modes are more frequently seen in the Dwarf-type in the present study.

As described in the preceding sections, SFHs of disk galaxies can be enhanced or reduced depending on model parameters. Therefore, it would be unrealistic for any theoretical studies on statistical properties of galactic SF to assume that irrespective of galaxy-masses, group/cluster masses, and orbital types, SF of galaxies in groups and cluster can be quenched after pericenter passage. The origin of passive red spiral galaxies observed in distant clusters (e.g., Dressler et al. 1998) can be closely related to the Quenched SF mode.

On the other hand, the origin of disk galaxies with local SF enhancement in their outer disks observed in the Virgo cluster (e.g., Koopmann & Kenney 2004) has something to do with the Enhanced SF mode.

### 3.5 A physical mechanism for enhanced SF

Although we have shown that SF in disk galaxies can be enhanced by ram pressure in the present simulations, we have only briefly mentioned a possible physical process responsible for this SF enhancement. In order to demonstrate more clearly why ram pressure can cause the modest enhancement of SF in disk galaxies, we investigate (i) the time evolution of gas densities (of SPH particles) and (ii) the density-temperature diagram of the particles during and after ram pressure stripping. We investigate these two points for gas particles that are finally converted into new stars, because it is meaningless for us to investigate these for all gas particles including stripped ones for the purpose of clarifying the physical mechanism of the derived SF enhancement. We choose the VI-II-MW-ED mode for this investigation, be-

cause the model clearly shows a SF enhancement. The SFH of this model is already described in Fig. 5 (as ‘Edge-on’ model).

Fig. 11 shows that the densities of star-forming gas particles significantly increase after the pericenter passage of the disk galaxy in this model. Fig. 11 furthermore shows that the locations of gas particles on the  $\rho_g - T$  plane after the pericenter passage are quite different from those in the isolated disk model. A significant fraction of gas particles can have higher  $\rho_g$  and higher  $T$  in the star-forming disk under ram pressure. These results confirm that the modest SF enhancement derived in the present simulations is due to the significant increase of gas densities caused by compression of gas by ram pressure of ICM.

### 3.6 Dependences on SN feedback effects and SF threshold gas densities

So far, we have presented the results of the models with a fixed  $\rho_{\text{th}}$  ( $=1 \text{ cm}^{-3}$ ) and  $t_{\text{adi}}$  ( $=10^6 \text{ yr}$ ). Although we consider that these parameter values for SF threshold gas density and SN feedback effect are quite reasonable and realistic for the present investigation, it is important for the present study to discuss whether or not the present results are sensitive to the choice of these parameters. We therefore discuss this point by presenting the results for the models (VI-II-MW-IN) with different  $\rho_{\text{th}}$  ( $=0.1 \text{ cm}^{-3}$  and  $1 \text{ cm}^{-3}$ ) and  $t_{\text{adi}}$  ( $3 \times 10^5 \text{ yr}$ ,  $10^6 \text{ yr}$  and  $10^7 \text{ yr}$ , which are referred to as ‘weak’, ‘standard’, and ‘strong’ SN feedback, respectively). The isolated models with these weak and strong SN feedback show significantly higher and lower initial SFRs than a reasonable SFR of  $\sim 1M_{\odot}$  for a MW-type disk galaxy, respectively. These models are therefore less realistic than those with the standard SN feedback ( $t_{\text{adi}} = 10^6 \text{ yr}$ ).

Fig. 12 shows that modest enhancement in SF after pericenter passage can be seen in the models with  $\rho_{\text{th}} = 0.1$  and  $1 \text{ cm}^{-3}$ , which confirms that the present results on the SF enhancement by ram pressure are not sensitive to the choice of  $\rho_{\text{th}}$ . Furthermore, Fig. 12 shows that SF enhancement can be seen in the model with strong SN feedback effects in which SN explosions can cause gaseous outflow from the disk galaxy. The SF enhancement can be clearly seen in the models with different  $t_{\text{adi}}$ , though the levels of SF enhancement are slightly different between the three models with weak, standard, and strong SN feedback. These results demonstrate that the present results on SF enhancement by ram pressure do not depend strongly on the details of the modeling of SN feedback effects.

## 4 DISCUSSION

### 4.1 SF enhancement in MW-type galaxies under ram pressure

We have shown that *in some models*, SF can be enhanced rather than truncated in MW-type disk galaxy when they pass the pericenter of their orbits within clusters. The high pressure of ICM can (externally) compress the cold ISM in disk galaxies so that SFRs, which are assumed to depend on local gas densities in the present study, can significantly

increase. Using analytic models of galaxy evolution in clusters, Fujita & Nagashima (1999) predicted that SFRs of disk galaxies can increase by a factor of  $\sim 2$  as galaxies approach the central regions of clusters, because ISM of the galaxies can be strongly compressed by high pressure of ICM at the pericenter passages. Previous numerical simulations also demonstrated that star formation in MW-type galaxies can be enhanced, if their ISM are under strong influences of high pressure of ICM (e.g., Bekki & Couch 2003; Kronberger et al. 2008). It should be stressed, however, that this SF enhancement in MW-type disk galaxies is modest (i.e., not like a starburst with a factor of  $\sim 10$  SFR increase) and can not last long. Such a modest level of SF enhancement in disk galaxies under ram pressure has been recently observed by integrated-field spectroscopy and multi-band imaging (e.g., Merluzzi et al. 2013).

The derived modest SF enhancement implies that SF in MW-type disk galaxies could not monotonically decline after they enter into cluster environments. Stripping of *halo gas* of disk galaxies by cluster tide (Bekki et al. 2001) and ram pressure of ICM (McCarthy et al. 2008; Bekki 2009) can cause gradual decline of their star formation (e.g., Larson et al. 1980). However, moderately strong ram pressure on *ISM in disks* can enhance star formation of disk galaxies in clusters: Cluster environments have positive and negative effects on galactic star formation histories. In recent semi-analytic models (SAMs) of galaxy formation based on a  $\Lambda$ CDM cosmology, star-formation quenching is assumed to occur in galaxies after their pericenter passages within groups and clusters (e.g., Wetzel et al. 2013). The present study strongly suggest that (i) galactic star formation in clusters is not so simple as modeled in these semi-analytic studies, and thus (ii) not only SF quenching but also SF enhancement would need to be correctly included in their models for better understanding galaxy evolution in clusters.

However, it is quantitatively unclear how dramatically the predictions of SAMs can change if the above ram pressure effects on SFRs of galaxies are more properly included in SAMs. Given that the SF enhancement by ram pressure is modest and a significant fraction of disk galaxies can have ‘unaffected’ SF modes after ram pressure stripping, such an inclusion of ram pressure effects in SAMs would not dramatically change the already existing predictions. Since SF enhancement means more rapid gas consumption, galaxies in groups/cluster might show reduced SF on average.

### 4.2 Environmental dependences of H $\alpha$ -to-optical-disk-size ratios

One of key results in the present study is that the final H $\alpha$ -to-optical-disk-size ratios ( $s_{\text{sf}}$ ) in disk galaxies under ram pressure of ICM depend primarily on their orbits (in particular, pericenter distances), galaxy masses, inclination angles of disks with respect to orbital directions, and cluster masses. Among these dependences of  $s_{\text{sf}}$ , an observable one is that disk galaxies are likely to show smaller  $s_{\text{sf}}$  in more massive clusters. This dependence of  $s_{\text{sf}}$  on  $M_{\text{h}}$  would not be so surprising and could be possibly confirmed by observations. However, systematic observational studies on the dependence of  $s_{\text{sf}}$  on  $M_{\text{h}}$  (or other cluster properties) have not been done yet. Koopmann & Kenny (2004) in-

investigated H $\alpha$  morphologies of spiral galaxies in the Virgo cluster and found that about 52% of the spiral galaxies show truncated H $\alpha$  disks (smaller  $s_{\text{sf}}$ ), particularly, in those with truncated H I disks (See their Fig. 15). They therefore concluded that the observed truncated SF regions in the Virgo can be caused by ISM-ICM hydrodynamical interaction.

Future observational studies on the dependences of  $s_{\text{sf}}$  on  $M_{\text{h}}$  (also on group/cluster sizes and densities) could be doubtlessly worthwhile as follows. Moss & Whittle (2000) investigated SF regions of disk galaxies in eight low-redshift Abell clusters and revealed that strong evidence for tidally induced star formation can be more frequently found in higher local galaxy surface density. Bretherton et al. (2013) have also found that disk galaxies with enhanced SFRs in their cluster samples show evidence of disturbance. These two observational studies imply that galaxy interaction can be also important in changing SF regions of galaxies in clusters and thus is a key parameter that controls  $s_{\text{sf}}$ . Therefore, a key question here is how the relative importance of ram pressure and tidal interaction in determining  $s_{\text{sf}}$  changes with galaxy environments (e.g.,  $M_{\text{h}}$ ).

The present study has shown that  $s_{\text{sf}}$  can be smaller for disk galaxies within more massive clusters, because ram pressure is likely to be stronger in the clusters. Also the reduction of  $s_{\text{sf}}$  can be less severe in groups than in clusters owing to the weaker ram pressure force in groups. On the other hand,  $s_{\text{sf}}$  is unlikely to be less than 1 during tidal interaction, because both gas and old stars within a certain tidal radius can be equally stripped. Furthermore slow yet strong galaxy interaction can be an important physical mechanism for enhancing rather than quenching SF in disk galaxies in groups (Bekki & Couch 2011). Therefore, it would be possible that (i) more massive clusters show a larger number of galaxies with smaller  $s_{\text{sf}}$  in comparison with less massive clusters and (ii) groups have different  $s_{\text{sf}}$  distributions in comparison with clusters (e.g., most of group member galaxies show  $s_{\text{sf}}$  almost equal to or larger than 1). Thus, future observational studies on the dependences of  $s_{\text{sf}}$  on group/cluster masses ( $M_{\text{h}}$ ) will enable us to understand the relative importance of ram pressure and tidal interaction in determining the 2D distributions of SF regions of disk galaxies in different environments.

### 4.3 Formation of disk E+As

The present study has shown that (i) low-mass disk galaxies can lose the entire gas disks through ram pressure stripping at their pericenter passage even in low-mass clusters with  $M_{\text{h}} = 10^{14}M_{\odot}$  and (ii) SF can be completely and suddenly truncated (or quenched) after the pericenter passage. SF is very active in these low-mass, gas-rich disk galaxies before SF quenching, and the stellar disk components can not be influenced at all by ram pressure stripping of ISM in these galaxies. Therefore, the present results imply that these low-mass disk galaxies which suddenly lose their gas can be identified as ‘E+A’ disk galaxies with poststarburst spectra 0.1 – 1 Gyr after SF quenching. Recent observational studies of spatial distributions of stellar populations and kinematics in E+As (e.g., Pracy et al. 2009; 2012) have shown that the observed properties of most E+As are consistent with the simulated ones based on a major merger scenario in which E+As can form from major merging with strong star-

bursts and evolve then into elliptical galaxies (e.g., Bekki et al. 2005). These results accordingly imply that disk E+As (i.e., those which are not formed from major merging) could be a minor population.

Although the observed negative radial gradients of Balmer absorption lines (i.e., stronger in inner regions) are demonstrated to be consistent with the major merger scenario of E+A formation (Pracy et al. 2012), some E+As show rather flat radial gradients of Balmer absorption lines (e.g., E+A 1 in Pracy et al. 2012). Disk galaxies which very quickly lose their entire gas disks through ram pressure stripping should show no/little radial gradients of Balmer absorption lines owing to sudden and complete truncation of SF for the entire disks. Therefore, the observed flat radial gradients of E+As in Pracy et al. (2012) appear to be consistent with E+A formation through ram pressure stripping in disk galaxies. Interestingly, E+A 1 in Pracy et al. (2012) has a dwarf-like luminosity ( $M_{\text{r}} = -16.7$  mag), which appears to be consistent with the present result that low-mass disks are more likely to become disk E+As. Given that Tran et al. (2003) found many disk E+As in clusters, the present study suggests that future observational studies on 2D distributions of Balmer absorption lines in disk E+As will enable us to discuss whether ram pressure stripping can be a major mechanism for E+A formation in clusters.

### 4.4 Timescale for SF quenching

The present study has clearly shown that SF quenching (i.e., complete truncation of SF) is possible in disk galaxies within groups and cluster for some models under some physical conditions (e.g., smaller  $r_{\text{p}}$  and lower galaxy masses). SF quenching has been demonstrated to occur in disk galaxies *at first pericenter passage* within clusters, as long as  $r_{\text{p}}$  is small enough ( $r_{\text{p}}$  well less than  $r_{\text{s}}$ ). Therefore, if the timescale for SF quenching is the time lag between when a galaxy first enters within a virial radius of its host cluster and when it passes through the orbital pericenter, then the timescale can be 2 – 3 Gyr for clusters. The present study has also shown that SF in the MW-type disk galaxies can not be completely truncated within 3.4 Gyr (during just once pericenter passage), if they have bound orbits (B1 and B2) with larger  $r_{\text{p}}$  in the high-mass clusters. It is, however, unclear whether SF in MW-type disk galaxies within clusters can be quenched if the galaxies can pass the pericenter twice or more.

We have investigated the long-term SFHs (5.6 Gyr) of disk galaxies with bound orbits (B1 and B2) for the Virgo model and the Coma one in order to understand whether SF quenching is possible for the MW-type disk galaxies with bound orbits and larger  $r_{\text{p}}$  in clusters. Fig. 13 shows that although SF quenching is not possible in the MW-type galaxies with bound orbits within 5.6 Gyr for the low-mass Virgo cluster model, dramatic SF reduction (almost SF quenching) is possible in the galaxies for the high-mass Coma model. This result implies that (i) SF quenching by ram pressure stripping is unlikely to occur in luminous disk galaxies for low-mass clusters and (ii) SF quenching timescale can be as long as  $\sim 6$  Gyr for luminous disk galaxies with larger  $r_{\text{p}}$  for high-mass clusters. Ram pressure stripping of cold gas from disk galaxies would not be the only mechanism of SF quenching within several Gyr for clusters, and tidal stripping due to galaxy interaction and cluster tide could be also

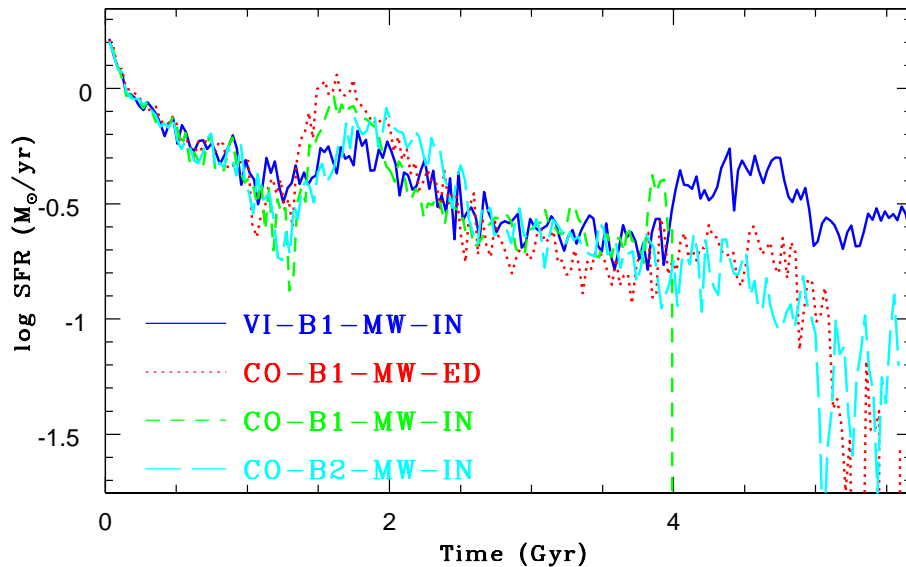


**Figure 13.** The long-time time evolution of SFRs in the four models, V1-B1-MW-IN (blue, solid), CO-B1-MW-ED (red, dotted), CO-B1-MW-IN (green short-dashed), and CO-B2-MW-IN (cyan, long-dashed). For these models, the MW-type disk galaxies can pass through orbital pericenter twice within the 5.6 Gyr orbital evolution. The CO-B1-MW-IN model shows a significant enhancement before SF quenching around  $T=4$  Gyr. This SF mode of ‘Enhancement before quenching’ can be seen in some models, though it is not a major mode.

responsible for SF quenching. It is thus our future study to investigate how ram pressure and tidal interaction can combine to quench SF in disk galaxies within clusters.

## 5 CONCLUSIONS

We have investigated the long-term SFHs (more than  $\sim 3$  Gyr) and the spatial distributions of SF regions of disk galaxies under strong ram pressure of ICM in clusters of galaxies by using numerical simulations with a new model for time-varying ram pressure force. The key parameters are (i) group/cluster halo masses ( $M_h$ ), (ii) pericenter distances of orbits ( $r_p$ ), (iii) inclination angles of disks with respect to the direction of their orbits ( $\theta$  and  $\phi$ ), and (iv) galaxy-types (e.g., MW-type). The principal results of the present numerical simulations are as follows.

(1) Ram pressure of ICM has the following three major effects on SFHs of disk galaxies in groups and clusters: (i) temporary and moderate enhancement of SF at pericenter passage, (ii) significant decline of SFRs after pericenter passage, (iii) complete truncation of SF (‘SF quenching’) after pericenter passage. It depends on  $M_h$ ,  $r_p$ , and  $\theta$  ( $\phi$ ) which of these three effects can be the most dominant for SFHs of galaxies in groups and clusters. It would be therefore unrealistic to adopt an assumption that SF of galaxies in groups and clusters can be uniformly shut down after pericenter passage in theoretical modeling on statistical properties of galactic SF and spectrophotometric properties in groups and clusters.

(2) SF enhancement by ram pressure is more likely to occur in MW-type disk galaxies, and the degree of SF

enhancement is more significant in the galaxies with lower inclination angles (e.g., edge-on configurations). However, such SF enhancement is only temporary (during and shortly after pericenter passage) and only modest (not like a factor of  $\sim 10$  increase in SFRs) in most cases. Less massive disk galaxies are less likely to show SF enhancement in clusters, because the entire gas disk can be stripped from less massive disks by even moderately strong ram pressure. SF enhancement by ram pressure can occur preferentially in the inner regions of disks, which implies that the inner mass densities can be slightly increased in disk galaxies under ram pressure.

(3) The dominant role of ram pressure in galactic SFHs is the significant reduction of overall SF in disk galaxies. The degree of SF decline depends strongly on group/cluster masses for a given set of galaxy parameters such that it can be more remarkable in groups and clusters with larger  $M_h$ . The level of SF decline by ram pressure can be more remarkable in less massive disk galaxies for a given group/cluster mass. Galaxies with smaller  $r_p$  show more severe SF decline in groups and clusters.

(4) Complete truncation of SF (‘quenching’) can occur in disk galaxies with different masses after pericenter passage in high-mass clusters ( $M_h = 10^{15}M_\odot$ ), as long as  $r_p$  is small enough ( $< r_s$ ). In low-mass clusters with  $M_h = 10^{14}M_\odot$ , SF quenching is unlikely to occur in MW-type disk galaxies owing to weaker ram pressure. These results imply that although the formation of anemic spirals is possible in low-mass clusters like the Virgo, the formation of passive spirals with no ongoing SF is unlikely in such clusters.

(5) Complete and sudden truncation of SF after

pericenter passage is more likely to occur in dwarf-like disk galaxies within groups and clusters. The likely outcome of this is that the galaxies can show poststarburst ('E+A') spectra characterized by strong Balmer absorption lines in the entire disks. The possible no/weak radial gradients of Balmer absorption lines in disk E+As with rotational kinematics is in striking contrast to the negative radial gradients observed in E+As formed from major galaxy merging. Thus, the present study predicts that (i) ram pressure can be responsible for the formation of disk E+As observed in clusters and (ii) disk E+As are likely to be dwarf-like disk galaxies.

(6) Ram pressure stripping of the outer gas disks of galaxies can significantly reduce the  $H\alpha$ -to-optical-disk-size ratios ( $s_{sf} = R_{sf}/R_s$ ) of the galaxies after pericenter passage. The level of  $s_{sf}$  reduction is likely to be more remarkable for disk galaxies in more massive clusters. The  $s_{sf}$  reduction also depends on  $M_h$  and  $r_p$  of disk galaxies for a given group/cluster mass and disk inclination angles ( $\theta$  and  $\phi$ ) such that it can be more remarkable for smaller  $M_h$  and smaller  $r_p$ . Such  $s_{sf}$  reduction can be seen for disk galaxies even in massive groups with  $M_h = 10^{13} M_\odot$  in which intragroup halo gas is warm rather than hot ( $T_{ICM} \sim 6 \times 10^6$  K). This result implies that SF regions can be also truncated (to a lesser degree) in group environment. Gas stripping by ram pressure can be efficient in groups and thus responsible for the lack of high H I mass galaxies observed in some groups (e.g., Kilborn et al. 2009).

(7) The global  $H\alpha$  morphologies corresponding to 2D distributions of SF regions in disk galaxies can be significantly changed by ram pressure. Disk galaxies under strong ram pressure can often show characteristic  $H\alpha$  morphologies, such as ring-like, one-sided, crescent-like, and highly asymmetric distributions. These results imply that 2D  $H\alpha$  distributions of disk galaxies can be used for revealing a physical effect of ram pressure on disk galaxies in groups and clusters.

## 6 ACKNOWLEDGMENT

I (Kenji Bekki; KB) am grateful to the referee for constructive and useful comments that improved this paper. Numerical simulations reported here were carried out on the three GPU clusters, Pleiades, Fornax, and gSTAR kindly made available by International Centre for radio astronomy research (ICRAR) at The University of Western Australia, iVEC, and the Center for Astrophysics and Supercomputing in the Swinburne University, respectively. This research was supported by resources awarded under the Astronomy Australia Ltd's ASTAC scheme on Swinburne with support from the Australian government. gSTAR is funded by Swinburne and the Australian Government's Education Investment Fund. KB acknowledges the financial support of the Australian Research Council throughout the course of this work.

## REFERENCES

- Abadi, M. G., Moore, B., Bower, R. G., 1999, MNRAS, 308, 947  
 Balogh, M. L., Navarro, J. F., Morris, S. L., 2000, ApJ, 540, 113  
 Bekki, K. 2009, MNRAS, 399, 2221  
 Bekki, K., 2013, MNRAS, 432, 2298  
 Bekki, K., Shioya, Y., 1998, ApJ, 497, 108  
 Bekki, K., Couch, W. J., Shioya, Y., 2001, PASJ, 53, 395  
 Bekki, K., Couch, W. J., Shioya, Y., 2002, ApJ, 577, 651  
 Bekki, K., Couch, W. J., 2003, ApJ, 596, L13  
 Bekki, K., Couch, W. J., Shioya, Y., Vazdekis, A., 2005, MNRAS, 359, 949  
 Bekki, K., Owers, M. S., Couch, W. J., 2010, ApJ, 718, L27  
 Bekki, K., Couch, W. J., 2011, MNRAS, 415, 1783  
 Boselli, A., Gavazzi, G., 2006, PASP, 118, 517  
 Bretherton, C. F., Moss, C., James, P. A., 2013, A&A, 553, 67  
 Brough, S., et al., 2013, MNRAS in press (arXiv:1308.2985)  
 Byrd, G. Valtonen, M., 1990, ApJ, 350, 89  
 Cortese, L., et al., 2012, A&A, 544, 101  
 Croom, S. M., et al., 2012, MNRAS, 421, 872  
 Crowl, H. H., Kenney, J. D. P., 2008, AJ, 136, 1623  
 Dressler, A., Oemler, A., Couch, W. J., Smail, I., Ellis, R. S., Barger, A., Butcher, H., Poggianti, B. M., Sharples, R. M., 1997, ApJ, 490, 577  
 Evrard, A. E., 1991, MNRAS, 248, p8  
 Fossati, M., et al. 2013, A&A, 553, 91  
 Fujita, Y., Nagashima, M., 1999, ApJ, 516, 619  
 Gunn, J. E., Gott, J. R. III., 1972, ApJ, 176, 1  
 Helsdon, S. F., Ponman, T. J., 2003, MNRAS, 339, L29  
 Jáchym, P., Palous, J., Köppen, J., Combes, F., 2007, A&A, 472, 5  
 Kennicutt, R. C. 1998, ApJ, 498, 541  
 Kilborn, V. A., Forbes, D. A., Barnes, D. G., Koribalski, B. S., Brough, S., Kern, K., 2009, MNRAS, 400, 1962  
 Koopmann, R. A., Kenney, J. D. P., 2004, ApJ, 613, 866  
 Kronberger, T., Kapferer, W., Ferrari, C., Unterguggenberger, S., Schindler, S., 2008, A&A, 481, 337  
 Larson, R. B., Tinsley, B. M., Caldwell, C. N., 1980, ApJ, 237, 692  
 McCarthy, I. G., Frenk, C. S., Font, A. S., Lacey, C. G., Bower, R. G., Mitchell, N. L., Balogh, M. L., Theuns, T., 2008, MNRAS, 383, 593  
 Mamon, G. A., 1992, ApJ, 401, L3  
 Mastropietro, C., Burkert, A., Moore, B., 2009, MNRAS, 399, 2004  
 Matsumoto, H., Tsuru, T. G., Fukazawa, Y., Hattori, M., Davis, D. S., 2000, PASJ, 52, 153  
 Merluzzi, P., et al. 2013, MNRAS, 429, 1747  
 Moore, B., Katz, N., Lake, G., Dressler, A., Oemler, A., 1996, Nat, 379, 613  
 Mori, M., Burkert, A., 2000, ApJ, 538, 559  
 Moss, C., Whittle, M., 2000, MNRAS, 317, 667  
 Navarro, J. F., Frenk, C. S., White, S. D. M., 1996, ApJ, 462, 563 (NFW)  
 Neto, A. F., 2007, MNRAS, 381, 1450  
 Ponman, T. J., Bourner, P. D. J., Ebeling, H., Böhringer, H., 1996, MNRAS, 283, 690  
 Pracy, M. B., Kuntschner, H., Couch, W. J., Blake, C., Bekki, K., Briggs, F., 2009, MNRAS, 396, 1349

- Pracy, M. B., Owers, M. S., Couch, W. J., Kuntschner, H., Bekki, K., Briggs, F., Lah, P., Zwaan, M., 2012, MNRAS, 420, 2232
- Quilis, V., Moore, B., Bower, R., 2000, Sci, 288, 1617
- Rasmussen, J., Ponman, T. J., 2007, MNRAS, 380, 1554
- Roediger, E., Hensler, G., 2005, A&A, 433, 875
- Roediger, E., Brüggem, M., 2007, MNRAS, 380, 1399
- Rosen, A., Bregman, J. N., 1995, ApJ, 440, 634
- Schulz, S., Struck, C., 2001, MNRAS, 328, 185
- Shioya, Y., Bekki, K., Couch, W. J., De Propris, R., 2002, ApJ, 565, 223
- Sutherland, R. S., Dopita, M. A., 1993, ApJS, 88, 253
- Thornton, K., Gaudlitz, M., Janka, H.-Th., Steinmetz, M., 1998, ApJ, 500, 95
- Tonnesen, S., Bryan, G. L., 2012, MNRAS, 422, 1609
- Vollmer, B., Cayatte, V., Balkowski, C., Duschl, W. J., 2001, ApJ, 561, 708
- Wetzel, A. R., Tinker, J. L., Conroy, C., van den Bosch, F. C., 2013, MNRAS, 432, 336

the SF. These results mean that the dependences of the present results on  $N_{\text{ICM}}$  and  $R_{\text{ICM}}$  are rather weak, as long as  $N_{\text{ICM}} \geq 40^3$  and  $R_{\text{ICM}} \geq 5R_s$ . Thus we consider that the present results for the models with  $N_d \sim 10^6$ ,  $N_{\text{ICM}} = 60^3$ , and  $R_{\text{ICM}} = 6R_s$  can be regarded as robust.

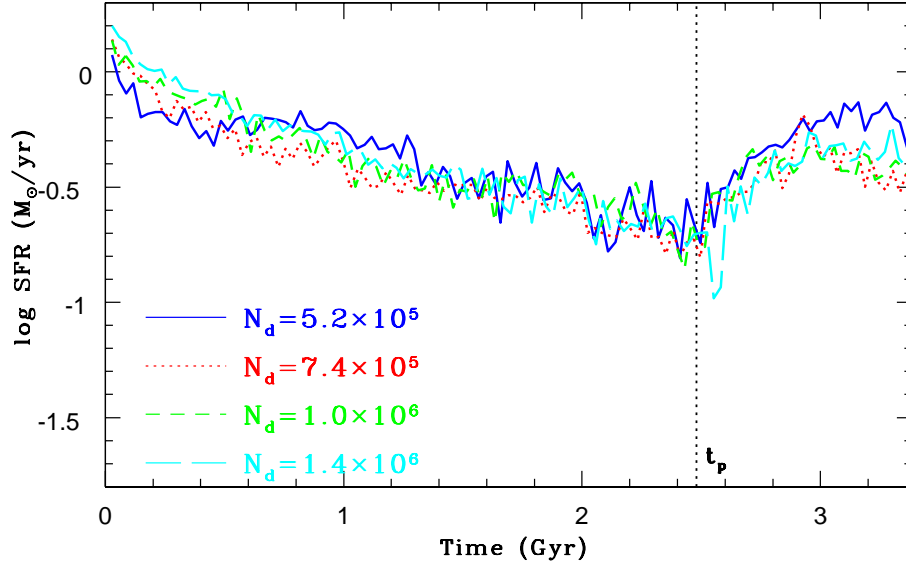
## APPENDIX A: RESOLUTION TEST

The present numerical results on the effects of ram pressure of ICM on the SFHs of disk galaxies could depend on the number of particles used for representing disk galaxies and ICM. Also, the sharp boundary of a ICM box could influence the details of hydrodynamical interaction between ICM and cold ISM in disk galaxies. Therefore, we here investigate how the present results depend on (i) the number of particles in a disk galaxy ( $N_d$ ), the number of ICM particles in a ICM box ( $N_{\text{ICM}}$ ), and the ICM box size ( $R_{\text{ICM}}$ ) by using models with different  $N_d$ ,  $N_{\text{ICM}}$ , and  $R_{\text{ICM}}$ . The models in which disks are under the strong influences of ram pressure are simply referred to as ram pressure models below.

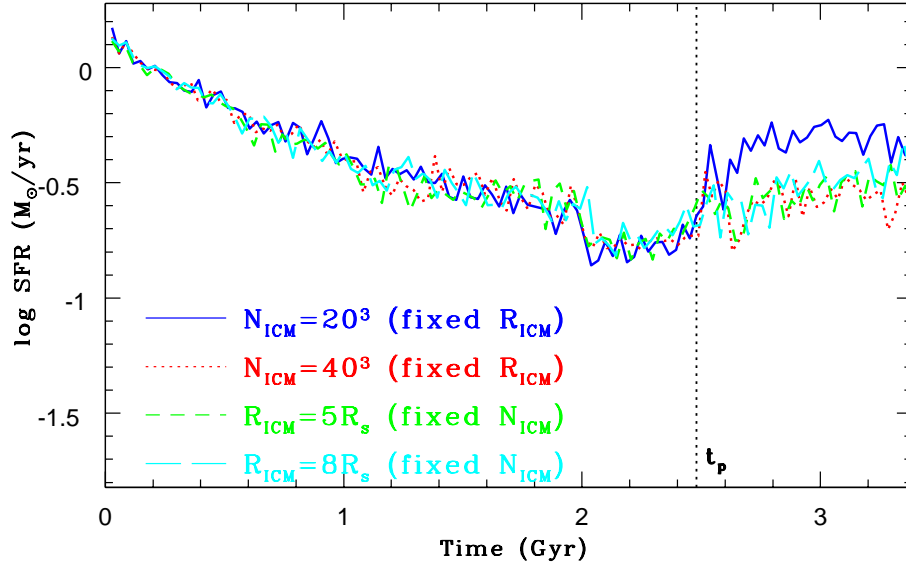
The VI-II-MW-IN model (‘inclined’ MW-type disk) is used for investigating the dependences of the present results on SF enhancement by ram pressure in disk galaxies on  $N_d$ , because this model clearly shows SF enhancement after pericenter passage. The VI-II-MW-FA model (‘face-on’ MW-type disk) is used for investigating how  $N_{\text{ICM}}$  and  $R_{\text{ICM}}$  change the hydrodynamical interaction processes between ICM and ISM and thus the SFRs, because the entire gas disk can be almost equally influenced by ram pressure force for this face-on model. The results for the models with different  $N_d$  and with different  $N_{\text{ICM}}$  and  $R_{\text{ICM}}$  are shown in Figs. 14 and 15, respectively.

Fig. A1 clearly shows that SF can be moderately enhanced by ram pressure in the ram pressure models for different  $N_d$ . Furthermore, the time evolution of SFRs is quantitatively similar between the four different ram pressure models, though the model with  $N_d = 5.2 \times 10^5$  shows a more strongly enhanced SF after pericenter passage. These results mean that as long as  $N_d$  is larger than  $\sim 7 \times 10^5$ , the present results on SFHs of disk galaxies in ram pressure models do not depend on  $N_d$ .

Fig. A2 shows that the time evolution of SFRs after pericenter passage is very similar between the models, except the low-resolution one with  $N_{\text{ICM}} = 20^3$ . More massive individual ICM particles in this low-resolution model ( $N_{\text{ICM}} = 20^3$ ) appear to compress more strongly the cold ISM of the disk and consequently enhance more significantly



**Figure A1.** The time evolution of SFRs in the MW-type disk galaxies with different total number of particles used for a disk ( $N_d$ ) and the same other parameters (VI-II-MW-IN models):  $N_d = 2.1 \times 10^5$  (blue, solid),  $N_d = 5.2 \times 10^5$  (red, dotted),  $N_d = 1.0 \times 10^6$  (green short-dashed), and  $N_d = 1.4 \times 10^6$  (cyan, long-dashed). The time at the pericenter passage is indicated by a black dotted line and marked with ' $t_p$ '.



**Figure A2.** The time evolution of SFRs in the MW-type disk galaxies with different total number of ICM particles ( $N_{\text{ICM}}$ ) and the ICM box size ( $R_{\text{ICM}}$  in units of  $R_s$ ) and the same other parameters (VI-II-MW-FA models):  $N_{\text{ICM}} = 20^3$  and  $R_{\text{ICM}} = 6$  (blue, solid),  $N_{\text{ICM}} = 40^3$  and  $R_{\text{ICM}} = 6$  (red, dotted),  $N_{\text{ICM}} = 40^3$  and  $R_{\text{ICM}} = 5$  (green short-dashed), and  $N_d = 40^3$  and  $R_{\text{ICM}} = 8$  (cyan, long-dashed). The time at the pericenter passage is indicated by a black dotted line and marked with ' $t_p$ '.